METHANE IGNITION IN A SHOCK TUBE WITH HIGH LEVELS OF CO_2 DILUTION

A Thesis

by

JOSHUA HARGIS

Submitted to the Office of Graduate and Professional Studies of
Texas A&M University
in partial fulfillment of the requirements for the degree of

MASTER OF SCIENCE

Chair of Committee,	Eric L. Petersen
Committee Members,	Timothy J. Jacobs
	Adonios N. Karpetis
Head of Department,	Andreas A. Polycarpou

May 2015

Major Subject: Mechanical Engineering

ABSTRACT

For decades Exhaust Gas Recirculation (EGR) has been used to mitigate several issues related to gas turbine operation: CO_2 sequestration; NO_x formation and emission; and combustor instabilities. EGR increases CO_2 concentrations in turbine exhaust for more efficient CO_2 scrubbing, reduces NO_x emissions, and reduces combustor instability associated with pressure resonances. As EGR technology has developed, EGR ratios have continued to increase and introduce greater amounts of combustion products, primarily CO_2, as part of the oxidizer in gas turbines. The goal of this study was twofold: to observe the role excess amounts of CO_2 play in causing non-idealities, bifurcation in particular, in shock-tube experiments using real (non-dilute) fuel-air mixtures, and to experimentally examine the kinetic effect, if any, of excess amounts of CO_2 as part of natural gas fuel-oxidizer mixtures.

Experiments were performed in a shock-tube facility on the campus of Texas A&M University. Mixtures were composed of a representative natural gas mixture at an equivalence ratio of $\phi = 0.5$ using modified oxidizer compositions representative of those used in EGR turbines. These oxidizer compositions maintained constant levels of O_2 while exchanging N_2 for CO_2 in stages to give oxidizer mixture concentrations ranging from ($0.21O_2$+$0.79N_2$) to ($0.21O_2$+$0.79CO_2$) with intermediate combinations of N_2/CO_2 in between. Low-pressure and high-pressure (near 1 atm and 10 atm, respectively) experiments were conducted over an approximate temperature range of 1450-1900 K for the simulated EGR mixtures. Upon conclusion of all experiments and

analyses, the observed effect of CO_2 relating to reflected-shock bifurcation was quite significant, giving stronger bifurcation as amounts of CO_2 increased, as determined by a sidewall pressure transducer. However, the observed kinetic effect of CO_2 on ignition delay time was quite small in comparing ignition delay times with and without CO_2. A modern chemical kinetics model also predicts that the effect of CO_2 dilution on methane ignition delay times at the conditions herein are very small, within the uncertainty of the experiments. This result helps to confirm the validity of the measured results. One can also conclude that despite the significant bifurcation and proportionately increased uncertainty in the test conditions as a result, the ignition delay time results herein seem to indicate that the test conditions are still at the nominal temperature and pressure as derived from the speed of the incident shock wave in the conventional way.

DEDICATION

I would like to dedicate this work to my mother and father for raising me to become the person I am and for their love and encouragement. I also would like to dedicate this thesis to my wife for being so patient and loving throughout this process.

ACKNOWLEDGMENTS

I would like to thank my committee chair, Dr. Petersen, and my committee members, Dr. Jacobs, and Dr. Karpetis, for their guidance and support throughout the course of this research.

Thanks also go to my friends and colleagues in the Petersen Research Group for assisting me in the lab and for their insights throughout the process of researching and writing this thesis.

Lastly, and most importantly, I would like to express my thankfulness to the Lord God who has greatly blessed me through his son, Jesus Christ, and for blessing me with the opportunity to work with such great people in the Petersen Research Group at this wonderful university.

NOMENCLATURE

EGR	Exhaust Gas Recirculation
CO_2	Carbon Dioxide (gaseous)
N_2	Diatomic Nitrogen
O_2	Diatomic Oxygen
CH_4	Methane
P_5	Pressure after passage of the reflected shock wave
T_5	Temperature after passage of the reflected shock wave
C_p	Specific Heat Capacity at Constant Pressure
γ	Ratio of Specific Heat Capacities (C_p/C_v)
x-t	Distance vs. Time
AST	Aerospace Shock Tube
HPST	High Pressure Shocks Tube

TABLE OF CONTENTS

Page

ABSTRACT ii

DEDICATION iv

ACKNOWLEDGMENTS v

NOMENCLATURE vi

TABLE OF CONTENTS vii

LIST OF FIGURES ix

LIST OF TABLES xii

CHAPTER

I INTRODUCTION 1

II EXPERIMENTAL SETUP 4

Facilities 5
Measurement Techniques and Configuration 7
Mixture Compositions and Experimental Conditions 11

III BACKGROUND ON NON-DILUTE MIXTURES IN SHOCK TUBES AND CO_2 IN COMBUSTION 14

Experimental Non-Idealities 14
Bifurcation 14
Brief Literature Review on Kinetic Effects of CO_2 25

IV RESULTS AND CONSEQUENCES OF HIGH CO_2 CONCENTRATION 27

Bifurcation 27
Decreased Energy Release 39
Effects on Ignition Delay Time and its Interpretation 48
Modeling Comparisons, Third-Body Effects of CO_2 58

V RECOMMENDATIONS AND FUTURE WORK 64

VI SUMMARY 67

REFERENCES 69

LIST OF FIGURES

Page

Figure 1. Mass fractions of CO_2 in turbine exhaust gas from two different levels of EGR. Figure re-created using data from [1]. 2

Figure 2. Standard x-t diagram during an experiment in a shock tube where the experiment is ended by the arrival of the expansion head at the test region near the endwall. 5

Figure 3. Shock-tube schematic showing dimensions for both the HPST and AST. 6

Figure 4. A typical optical setup used to measure chemiluminescence from sidewall and endwall ports in a shock tube. 7

Figure 5. a) Example time histories of endwall pressure and sidewall pressure and emission traces used to calculate ignition delay time in dilute mixtures (99.1% dilution in Ar). b) Definition of time zero is defined by the arrival of the reflected shock wave at the sidewall pressure transducer. 9

Figure 6. Example time histories of endwall pressure and sidewall pressure and emission traces from Mix 1 (Table 1). a) Example of method used to calculate ignition delay time in non-dilute mixtures. b) Definition of time zero is defined by the arrival of the reflected shock wave at the sidewall pressure transducer. 10

Figure 7. Example of reflected-shock bifurcation in a shock-tube experiment with an ideal pressure trace (all transducers have zero diameter). Taken directly from [10]. 17

Figure 8. Local ignition behind reflected shock waves with bifurcation. Ignition along sidewall is evident from these schlieren images. Non-dilute C_2H_2-O_2 mixture at 1031 K, 1 atm. Taken directly from [25] with copyright permission from Elsevier B.V. 21

Figure 9. x-t diagram schematics of contact surface interaction with the reflected shock wave in a shock-tube experiment. a) Reflected expansion. b) Reflected compression. 23

Figure 10. Pressure traces showing time zero defined from the endwall and bifurcation passage over sidewall pressure transducer to define the length of a bifurcation. 29

Figure 11. Sidewall pressure traces showing bifurcation behavior at the sidewall pressure transducer for the 4 hot flow mixtures in the AST at low pressures and similar temperature conditions. Note that the traces have

been shifted so that the arrival of the bifurcated foot occurs at time zero. Also, these are purely flow effects with no ignition taking place. 30

Figure 12. Bifurcation magnitude for each mixture in the AST at low pressures (~1 atm).....31

Figure 13. Sidewall pressure traces showing bifurcation behavior at the sidewall pressure transducer for Mix 1 and Mix 4 in the AST at low pressures and similar temperature conditions. Note that the traces have been shifted so that the arrival of the bifurcated foot occurs at time zero. Also, these are purely flow effects with no ignition taking place.....32

Figure 14. Bifurcation magnitude for Mix 1 and Mix 4 in the HPST at high pressures (~10 atm). 32

Figure 15. Bifurcation magnitude in terms of time span for all hot flow mixtures in both the AST and HPST.....33

Figure 16. Variation in pressure oscillations as a result of bifurcation for the hot mixtures in the AST at one T_5 condition. These are purely flow effects with no ignition taking place. 36

Figure 17. Variation in pressure oscillations as a result of bifurcation for the cold mixtures (2'-4') in the AST.....37

Figure 18. Variation in pressure noise as a result of bifurcation for Mix 1 and 4 in the HPST. These features are purely flow effects with no ignition taking place. 38

Figure 19. Variation in pressure noise as a result of bifurcation for cold mixture in the HPST. 38

Figure 20. Pressure and emission traces of Mix 1-4 in AST with suppressed ignition levels in the endwall pressure trace. The endwall pressure transducer is the primary ignition diagnostic in these traces. Ignition regions are circled. 40

Figure 21. Pressure and temperature increase during CHEMKIN simulation of ignition delay in Mix 1 and Mix 4.....42

Figure 22. Pressure and emission traces from hot-flow experiments showing the pressure expansion behavior (in circles). The endwall pressure data in the graphs have been shifted down to give a clearer view of the traces.....44

Figure 23. Cold flow for Mix 2'-4' in the AST. The pressure discontinuity grows more noticeable with increasing CO_2 content. As in Figure 22, the endwall data have been shifted down for easier viewing. 45

Figure 24. Mix 1 and Mix 4 in the HPST. The pressure drop-off is seen in Mix 4, but not in Mix 1. 46

Figure 25. Example of the pressure discontinuity in the HPST for Mix 4' (cold flow). 46

Figure 26. Cold flow in Mix 2', showing a pressure rise at a high T_5 instead of a drop-off like at lower temperatures. 47

Figure 27. Intersecting slope method for mixtures with more CO_2, all near a common T_5. 49

Figure 28. Method for defining ignition delay time in mixtures with noisy pressure traces and suppressed ignition pressure rise. a) Two intersecting slopes define the time of ignition, b) Because of non-quiescent conditions additional uncertainty in ignition time is introduced (shown with three possible times). c) The last figure has no emission to more clearly show the range of uncertainty. 50

Figure 29. Experiments conducted in the HPST near 10 atm. Even with an endwall diagnostic, interpreting ignition delay is still a challenge in Mix 4. 51

Figure 30. Ignition delay times for each mixture at 1.75 atm, shown compared to Mix 1 on an individual basis, then together. a) Mix 1 vs Mix 2, b) Mix 1 vs Mix 3, c) Mix 1 vs Mix 4, d) All mixtures. The model referred to in the graphs is the Aramco 1.3 mechanism from NUIG. 53

Figure 31. Ignition delay times for experiments in the HPST at 10 atm. 55

Figure 32. Ignition delay time data for all mixtures in the AST at 1.75 atm. Included for comparison are the discarded data from the experiments with a pressure drop-off (the open boxes). 57

Figure 33. Ignition delay time data for all Mix 1 and 4 in the HPST at 10 atm. Included are the discarded data from the experiments with a pressure drop-off (the open boxes). 58

Figure 34. Modeling comparisons of third-body collision efficiencies for Mix 1 and Mix 4 at 1.75 atm. 62

Figure 35. Modeling comparisons of third-body collision efficiencies for Mix 1 and 4 at 10 atm. 63

LIST OF TABLES

Page

Table 1. The four different mixtures investigated in this study at an equivalence ratio of ϕ=0.5.....12

Table 2. Cold flow mixtures representative of Mixtures 2-4, but without fuel or oxidizer.....13

CHAPTER I

INTRODUCTION

As the gas turbine industry continues to grow and change, research focused on this industry must keep pace and do the same. Although gas turbines utilizing exhaust gas recirculation (EGR), also referred to as flue gas recirculation, have been in use for several decades, the configurations used in such turbines have also evolved ([1], [2]). Likewise, investigations into gas turbine fuels have varied widely, ranging from typical methane-air mixtures, as in [3], to more complex mixtures as in [4]. Additionally, higher EGR rates introduce larger amounts of CO_2, prompting study of mixtures with higher CO_2 concentrations. Figure 1 shows data from [1], displaying higher CO_2 concentrations in turbine exhaust gas as a direct result of higher EGR ratios.

A natural extension for chemical kinetics studies involving EGR-based mixtures, those conducted in shock tubes in this case, is to expand the scope of the study to include greater amounts of CO_2 than even the highest EGR ratios in modern gas turbine systems. While much data based on methane ignition in shock tubes exists in the literature, little was found by the author that included high or even moderate amounts of CO_2 as a component in non-dilute shock-tube mixtures using methane as a fuel (non-dilute mixtures refer to those at typical mixtures representative of fuel-air mixtures with about 70-75% N_2, as opposed to mixtures with much larger percentages of N_2 or Ar gas). This state of affairs comes as no surprise however, considering the inherent difficulties of performing experiments in non-dilute mixtures with CO_2 as a major constituent. Thus

comes the motivation of this thesis: to study the ignition of methane in shock tubes with high amounts of CO_2 in non-dilute mixtures.

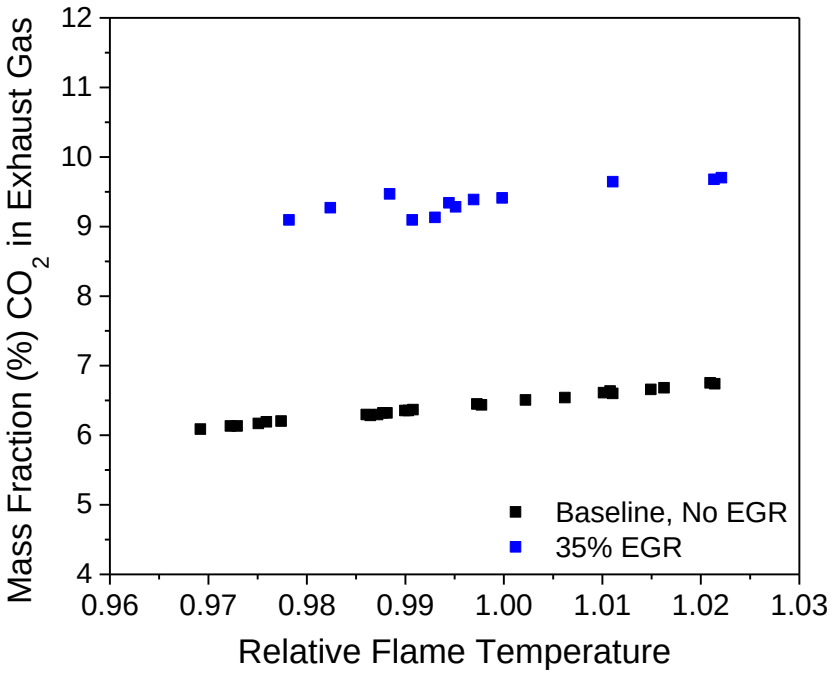

Figure 1. Mass fractions of CO_2 in turbine exhaust gas from two different levels of EGR. Figure re-created using data from [1].

This thesis is organized into separate chapters and follows the style guide of the *American Society of Mechanical Engineers*. This chapter, Chapter I, is the introduction. Chapter II provides details on the experimental setup, which consists of the facilities involved, measurement configurations and techniques used, and the mixture compositions and experimental conditions tested in this study. Chapter III discusses the challenges of performing shock-tube experiments associated with non-dilute mixtures. Chapter IV presents the results of the experiments, including difficulties encountered

during the data collection and analysis. Recommendations for improvement and future work are included in Chapter V. Finally, Chapter VI gives a brief conclusion of the experiments and results discussed in this thesis.

CHAPTER II

EXPERIMENTAL SETUP

A typical shock-tube setup consists of two sealed tube sections separated by an impermeable diaphragm assembly. One section is filled with a high-pressure gas, usually helium, and is referred to as the driver section (this drives the shock). The other is referred to as the driven section and is filled to low pressure with whatever test gas is being studied. In the case of this thesis, the test gas in the driven section was composed of CH_4, O_2, and a combination of N_2 and/or CO_2. To conduct an experiment using polycarbonate diaphragms, the driver side is filled until the diaphragm makes contact with a cutter (for repeatability of experiments) and bursts. Once the diaphragm is ruptured, a shock wave forms due to the large pressure differential between the two sections and travels towards the driven end of the tube. An expansion head also forms and travels toward the driver end of the tube. The shock wave propagates down the driven section of the tube and reflects off the endwall. When the shock reaches the endwall, this denotes the beginning of the experiment. The expansion head eventually reflects from the wall in the driver section and heads toward the driven side of the tube. Additionally, an interface between the driver and driven gases, known as the contact surface (or more accurately, contact region), follows the incident shock wave toward the driven side of the tube. At some point after the incident shock reaches the endwall and reflects, it interacts with either the expansion head or contact surface, and an expansion wave (or in some cases a pressure wave) is sent toward the endwall. Once this

disturbance reaches the endwall, the test time is over. During this test time, the goal of kinetics measurements is for a reaction to have occurred and measurements to have taken place. Usually reactions occur prior to arrival of the contact surface/expansion head, however there are occasions in which they do not, such as in experiments at too low of a temperature, or fuels with lower reactivity. Figure 2 presents an x-t diagram during a typical shock-tube experiment.

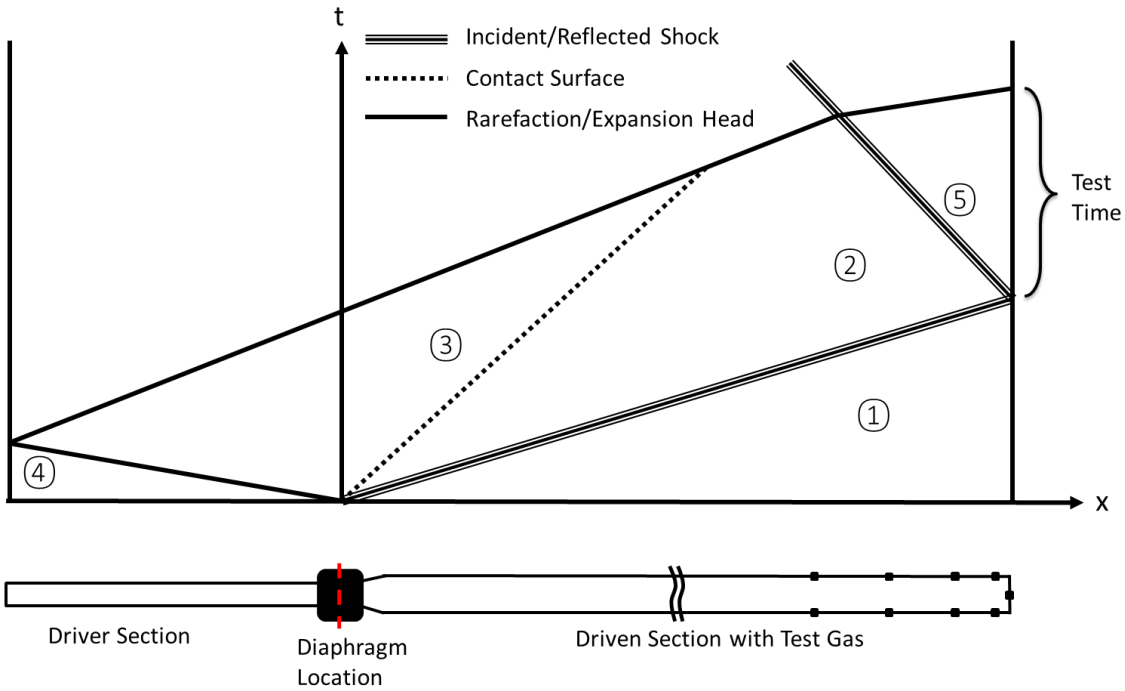

Figure 2. Standard x-t diagram during an experiment in a shock tube where the experiment is ended by the arrival of the expansion head at the test region near the endwall.

Facilities

For the experiments conducted in this work, two state-of-the-art shock-tube facilities were used to perform chemical kinetics experiments. Both facilities can be used

for measurements relating to dilute and non-dilute mixtures and are shown schematically in Figure 3. The facilities are located on the campus of Texas A&M University in the Turbomachinery Laboratory.

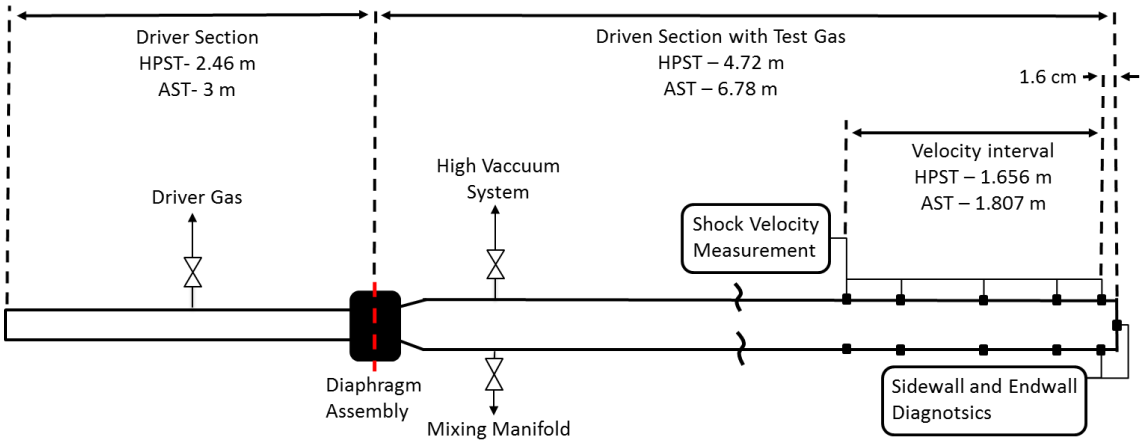

Figure 3. Shock-tube schematic showing dimensions for both the HPST and AST.

The first shock tube, as described in [5], was acquired in 2008, and the second, as described in [6] and [7], was generously donated by Aerospace Corporation in El Segundo, CA in 2013. The first tube's purpose is focused on high-pressure experiments in both dilute and non-dilute kinetics experiments, and is thusly referred to as the High Pressure Shock Tube (HPST). The second tube from Aerospace Corporation is referred to as the Aerospace Shock Tube (AST), and is currently used for the study of lower-pressure and dilute chemical kinetics. Both tubes are made from stainless steel and have an inner diameter of approximately 6 inches, combined with mirror-finish sidewalls to minimize boundary layer effects. Additionally, the tubes are equipped with 5 PCB 113B22 pressure transducers along the driven tube to determine incident shock speed.

An additional PCB transducer is placed at the endwall to record time histories of reflected-shock pressure. Time histories of experimental pressure on the sidewall are also recorded by a Kistler 601B1 transducer at a location 1.6 cm from the endwall. The shock tubes are also equipped with viewing ports on the endwall and sidewall for either laser absorption or chemiluminescence measurements, as shown in Figure 4.

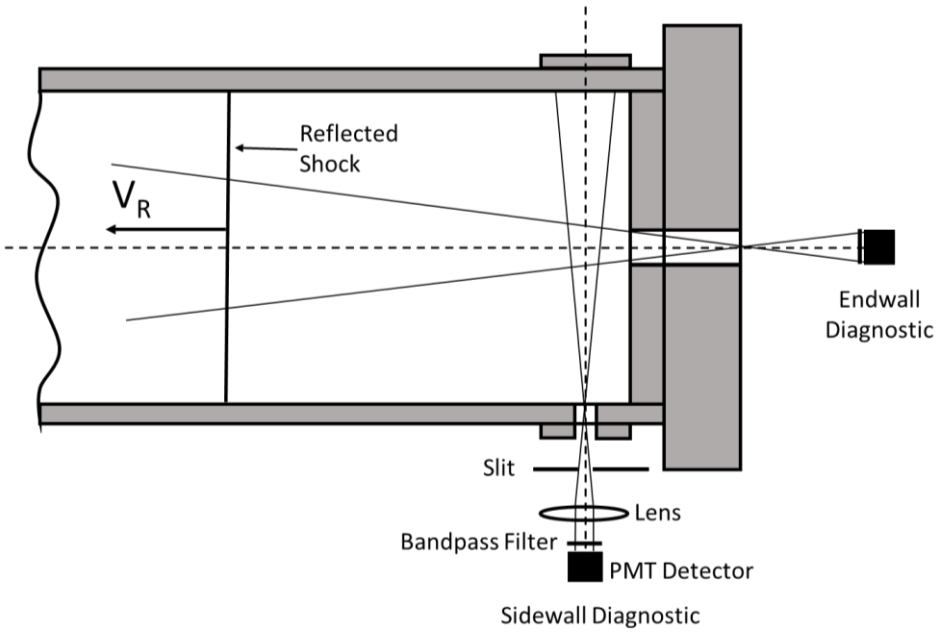

Figure 4. A typical optical setup used to measure chemiluminescence from sidewall and endwall ports in a shock tube.

Measurement Techniques and Configuration

Prior to collecting data from experiments, the accuracy of the reflected-shock conditions in the shock tubes must be verified. References [5]-[7] discuss the validity of the reflected-shock conditions and verify that the uncertainty of conditions, particularly

in T_5, in each tube are acceptable. For the HPST, the uncertainty in T_5 conditions is less than 10 K, and for the AST uncertainty in T_5 is also less than 10 K, up to a reflected-shock temperature of 2200 K. This level of precision is the case for both tubes because each has been optimized for the spacing of pressure transducers along the tube length to minimize uncertainty in incident-shock velocity measurement. Since incident-shock attenuation is nearly linear over the velocity measurement region (as discussed in [5] and [7]) and the last measurement interval is very near to the endwall (see Figure 3), the shock velocity can accurately be extrapolated to the endwall. Making use of the well-known normal-shock (NS) relations, conditions behind the reflected shock wave can be calculated from the extrapolated incident-shock velocity. Because of the small uncertainty in incident-shock velocity, it was discussed in [5] and [7] that when using the last velocity interval compared to the whole range of velocity for incident-shock velocity, the difference in calculated T_5 from the NS relations was the primary source of uncertainty in T_5, which was less than 10 K.

In addition to diagnostics for shock velocity measurements along the tube, diagnostics near the endwall of the tube are used to record time histories of pressure and chemiluminescence from excited species, such as OH* and CH*. As discussed in [8], experiments performed under dilute conditions benefit from increased accuracy of sidewall pressure and emission diagnostics, while those performed under non-dilute conditions are better suited to diagnostics located at the endwall of the shock tube. Figure 5 shows time histories of pressure and emission in a dilute experiment, which are used to calculate the ignition delay time of a shock-heated mixture. In general, ignition

delay time is a fairly intuitive concept, but is defined differently in dilute and non-dilute mixtures. In dilute experiments, ignition delay time is defined as the time from reflected-shock arrival at the sidewall measurement location, to the time of zero emission intersection of a tangent line from the steepest slope of the sidewall emission profile. This definition can be better understood when again examining Figure 5. In non-dilute experiments, ignition delay time is defined as the time between incident-shock arrival at the endwall and the time of the initial, sharp pressure rise of the endwall pressure trace. An example of ignition delay time in non-dilute mixtures can be observed in Figure 6. For clarification, the beginning of experiments (time zero) is defined differently for experiments in dilute and non-dilute mixtures. This difference can be seen by comparing Figure 5 b) with Figure 6 b).

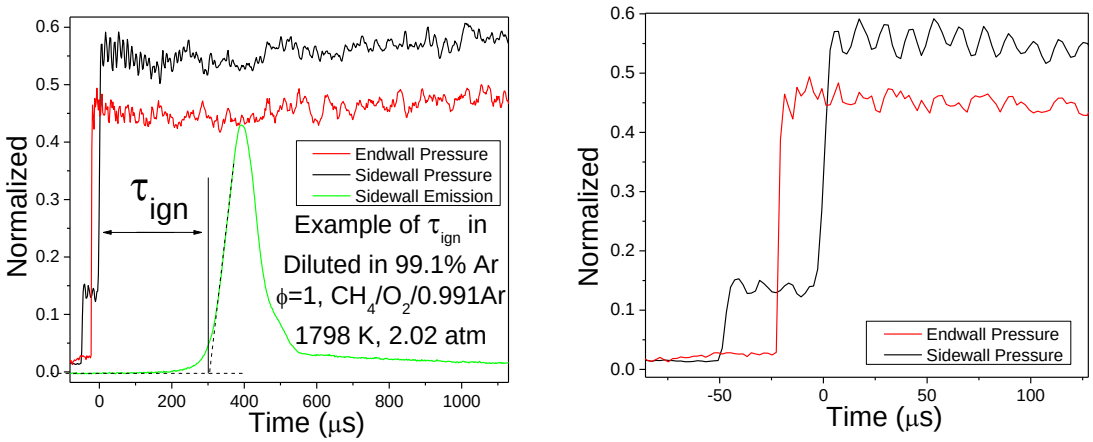

Figure 5. a) Example time histories of endwall pressure and sidewall pressure and emission traces used to calculate ignition delay time in dilute mixtures (99.1% dilution in Ar). b) Definition of time zero is defined by the arrival of the reflected shock wave at the sidewall pressure transducer.

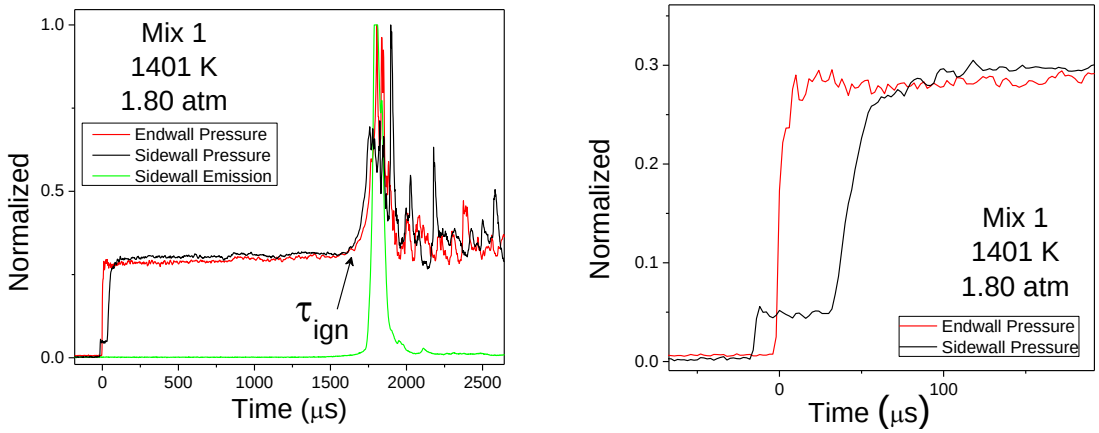

Figure 6. Example time histories of endwall pressure and sidewall pressure and emission traces from Mix 1 (

Table 1). a) Example of method used to calculate ignition delay time in non-dilute mixtures. b) Definition of time zero is defined by the arrival of the reflected shock wave at the sidewall pressure transducer.

Since the experiments performed in this study were focused on non-dilute mixtures, endwall diagnostics were the primary tool used. In the case of the AST, only a pressure diagnostic was available at the endwall, and no emission endwall diagnostics were used. However, as the mixtures investigated were highly reactive, pressure diagnostics were assumed to be satisfactory in determining ignition at the endwall, as was investigated previously in [8] for real fuel-air mixtures under non-dilute conditions. This use of pressure rise for ignition was shown to be a good assumption while conducting this study, though an endwall emission diagnostic would have been beneficial had it been available for the AST facility. However, the more tools an experimenter can use to collect information about an experiment, the better. It is shown in a later section that even though the endwall pressure trace is the most useful tool in determining ignition delay time (to be defined in a subsequent paragraph) for these

mixtures, the pressure traces were observed to be inherently noisy due to the effects of bifurcation.

Mixture Compositions and Experimental Conditions

As the goal of this study was to investigate mixtures typical of those used in gas turbines, and then introduce high concentrations of CO_2, a lean mixture of methane and air was used as the baseline mixture. For subsequent mixtures, the equivalence ratio was held constant, while varying the amount of N_2, exchanging it with equivalent amounts of CO_2.

Table 1 shows the mixture compositions, all at an equivalence ratio of $\phi = 0.5$, investigated in this study. Each mixture was tested at average pressures of 1.75 atm and 10 atm, respectively, and at temperatures ranging from approximately 1400 K to 1900 K. Due to the known pressure dependence of methane-based fuel mixtures [3], only Mixtures 1 and 4 were tested at higher pressures near 10 atm, while all mixtures were tested at the lower average pressure of 1.75 atm. To be sure of the baseline mixture at 10 atm, results from this study were also compared to those of a previous study [3]. In addition to mixtures with fuel, 3 additional mixtures were used to mimic the flow behavior of Mix 2, 3, and 4, respectively without any chemical reactions. These additional mixtures were comprised solely of CO_2 and N_2 in ratios similar to those in the mixtures with CH_4 and O_2. Since the additional mixtures had no fuel or oxidizer, they

were un-reacting, and are thus referred to as "cold," while the reacting mixtures with CH_4 and O_2 are referred to as "hot." The cold flow mixtures are hence designated with a prime associated with the mixture name, such as Mix 2'. The cold flow mixtures are shown in Table 2.

To make mixtures for experiments, the AST and HPST are equipped with a gas-handling manifold and mixing tank for each tube. The manifold consists of a series of valves and pressure transducers to monitor pressure in the manifold during mixture preparation. Mixtures are made using the partial pressure method, where the mole fractions of each species are known within 1% uncertainty, at worst. The uncertainty of the true fuel-oxygen equivalence ratio is usually much less than this. Since components with lower mole fractions in a mixture are filled first (this usually being the fuel and oxygen, along with other small additives as necessary), the total pressures are low, which enable the use of more sensitive pressure transducers. The low-pressure transducers have an accuracy of 0.1 torr up to 1000 torr, while for pressures above 1000 torr, the accuracy is within 0.1 psi.

Table 1. The four different mixtures investigated in this study at an equivalence ratio of ϕ=0.5.

Mixture	CH_4	O_2	CO_2	N_2
1 (Baseline)	0.05	0.20	0.00	0.75
2	0.05	0.20	0.25	0.50
3	0.05	0.20	0.50	0.25
4	0.05	0.20	0.75	0.00

Table 2. Cold flow mixtures representative of Mixtures 2-4, but without fuel or oxidizer.

Mixture	CO_2	N_2
2’	0.74	0.26
3’	0.47	0.53
4’	0.21	0.79

CHAPTER III

BACKGROUND ON NON-DILUTE MIXTURES IN SHOCK TUBES AND CO_2 IN COMBUSTION

Experimental Non-Idealities

The study of chemical kinetics is aided by the fact that most reactions occur very quickly, allowing the use of vessels that can attain high pressures and temperatures for brief periods of time. Though shock tubes are intended to produce an ideal environment for combustion kinetics experiments, they are not perfect. Even in relatively simple experiments, like those conducted in dilute conditions, care must be taken before and during the experiments to prevent non-idealities from interfering with the data. For non-dilute mixtures containing large amounts of diatomic and polyatomic species, as in the case of this study, several non-idealities present themselves during the course of an experiment. Using proper measurement equipment and techniques, some of these non-idealities can be overcome or, at worst, dealt with during the experimental process. Others cannot be overcome and must be taken into consideration and worked around. Of the non-idealities encountered and investigated in this study, reflected-shock bifurcation and its effects are the primary concerns.

Bifurcation

To achieve ideal conditions in a shock tube, researchers often use a monatomic bath gas, such as Argon. Though dilute mixtures are useful in determining finer kinetic

behaviors of gases since the resulting temperature time histories are relatively constant, the use of non-dilute mixtures are often required to gain an understanding of the interactions that occur in realistic fuel-air mixtures. When a diatomic bath gas, such as naturally occurring Nitrogen, is used in shock-tube experiments, the boundary layers lack the momentum needed to pass through the normal portion of the shock wave and interact to a greater degree than those in a bath gas composed primarily of Argon. Similarly, mixtures with CO_2 also have energy-deficient boundary layers. This energy deficiency occurs based on the composition of the test gas. In a shock-fixed coordinate frame, the relation between total pressure in the boundary layer and in the reflected-shock is what determines the presence of bifurcation. Mark [9] showed in the original theory that the total pressure in the boundary layer depends only on the incident Mach number and specific heat ratio of the gas (which is composition-dependent). While boundary-layer growth itself causes some issues, it is the interaction of the reflected shock with the boundary layer that is of key interest.

When a reflected shock wave propagates back into a shock-tube flow in which energy-deficient boundary layers are present, a phenomenon known as reflected-shock bifurcation occurs. Shock-wave bifurcation presents itself in the form of a lambda-shaped shockwave (as in the Greek letter, λ). Figure 7 shows a schematic of reflected-shock bifurcation. Bifurcation of the reflected shock wave occurs when the fluid in the boundary layer does not have enough momentum to pass through the shock, in shock-fixed coordinates. Since the boundary-layer fluid doesn't pass through the reflected shock, it is pushed along in front of the shock – forming compression waves. These

compression waves then coalesce into a curved or oblique shock. The energy-deficient boundary layer fluid then passes under the shock and builds up underneath the oblique portion of the reflected shock. This phenomenon occurs when $P_{0,bl}/P_2 < P_5/P_2$ [9]. As the original oblique shock is formed to minimize total pressure loss, a second is formed to return the flow parallel to the wall of the shock tube. Once the flow passes through the second oblique shock, its velocity along the axis of the tube is non-zero, unlike the velocity passing through the normal portion of the shock wave, causing a slip line (or vortex sheet) to form from the interaction of the moving and stationary fluids. The pressure after the second oblique shock continues to rise until the passage of the stagnation streamline, where the pressure then drops to that of the gas that passed through the normal portion of the shock wave. Naturally, this process can mask the arrival of the normal portion of the reflected shock wave (shown by the ideal pressure trace in Figure 7). It can also induce a great amount of vorticity, and, more importantly, it can result in a non-uniform flow field behind the reflected shock wave. For these reasons, great care must be taken in the interpretation of pressure traces behind reflected shock waves in diatomic and polyatomic gases as well as the determination of the post-shock experimental conditions pertinent to the kinetics study being undertaken.

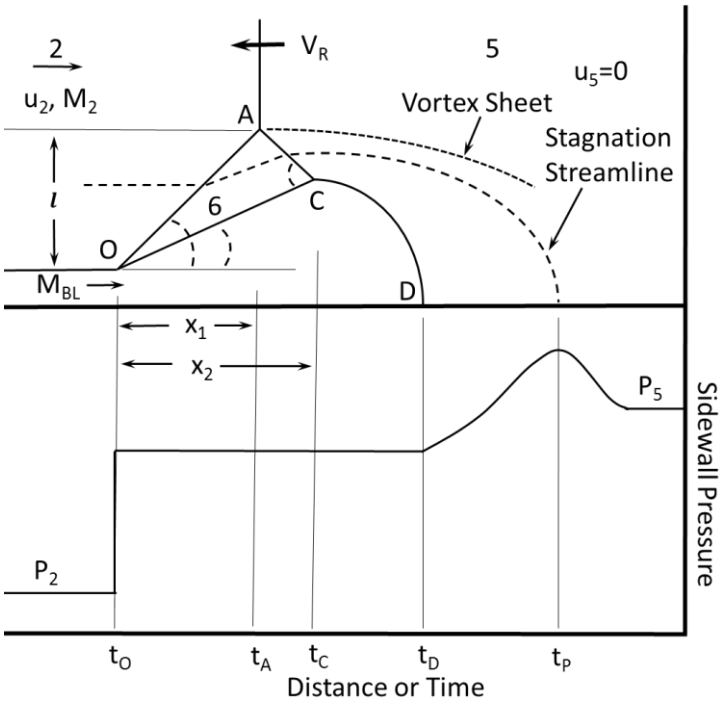

Figure 7. Example of reflected-shock bifurcation in a shock-tube experiment with an ideal pressure trace (all transducers have zero diameter).

Prior Work

Bifurcation was first observed by Mark [9] in 1958. In [9], Mark discusses the propagation of a reflected shock wave in a shock tube where the gas behind the incident shock has a non-uniform flow field (a boundary layer) due to viscous effects. In that work, the basic criteria for reflected-shock bifurcation (discussed in the previous paragraph) are laid out as the result of several experiments (conducted mostly with air). In addition to discussing the criteria for bifurcation, Mark also discusses the range of conditions over which bifurcation occurs in relation to gas composition (γ) and incident Mach number. Mark's work was followed by that of Strehlow and Cohen shortly after [11], which investigated the implications of bifurcation relating to chemical kinetics

measurements. Like Mark, Strehlow and Cohen made use of schlieren imaging to capture the behavior of bifurcated reflected shocks, but also made note of how the density gradients observed by the images were indicative of temperature gradients within the flow, leading to conclusions that non-uniform temperature regions existed near the tube walls after the bifurcation. Further work was done by Byron and Rott [12], extending the model of Mark to explain the entrainment of the boundary layer under the bifurcated foot of the reflected shock wave. Further, Center [13] made use of piezoelectric transducers to capture the pressure behavior of bifurcations near the sidewall of a shock tube, agreeing with the works of [9] and [12]. Though much experimental progress was made in the way of discovering and understanding reflected-shock bifurcation in the middle of the 20th century, progress has continued in the investigation and understanding of this phenomenon since that time [14-17]. More recently, Petersen and Hanson investigated the bifurcation effect at pressures much higher than previously studied [10]. They found that, for pressures ranging from near 11-265 atm, pressure had almost no effect on observed bifurcation features, such as height and length of the bifurcation. Additionally, Petersen and Hanson confirmed the influence of mixture composition on the bifurcation features, like the pioneering work of Mark (though over a much wider range of conditions and compositions). Along with the experimental works just mentioned, numerous numerical investigations into the nature of reflected-shock bifurcations have taken place.

As with experimental techniques, numerical techniques simulating fluid flow have aided in the understanding and investigation of bifurcation in shock tubes. In [18],

Takano was able to partially resolve the front leg of bifurcation features, as well as flow disruptions indicative of a separation bubble, using 2-D finite-difference Navier-Stokes solvers. With advances in computing power a few years later, Kleine et al. were able to better resolve the front leg and separation bubble of a bifurcated shock wave using a grid-adaptation technique, MacCormack's method [19]. Included in that same work are experimental results using the color-schlieren technique to visualize the bifurcation behaviors in CO_2-rich flows. Just as their computational results were a step forward in resolving bifurcations numerically, the experimental results of Kleine et al. from the color schlieren setup were a step forward in the conceptual understanding of bifurcated flow fields in shock tubes.

With the improvement of methods in [19] over those in [18], Nishida and Lee's work was a further improvement, capturing a majority of the features of the bifurcation, including the front shock and separation bubble along with the vortex sheet and even a partial curling of the vortex sheet at the endwall. These were groundbreaking works in the field of numerical schemes to simulate reflected-shock bifurcation, with advances continuing [20, 21] into what is now modern computational fluid dynamics (CFD). Recent researchers [22-24] give a small glimpse into the application of CFD for simulations involving bifurcations. These modern CFD simulations capture much of the behavior observed from past experimenters regarding reflected-shock bifurcation. Not only have the results of these CFD simulations been confirmed when compared to experiments, they have also provided valuable insight into the behaviors of the flow beyond experimental observations.

Influence of Flow Effects on Combustion Chemistry

Like other modern CFD computations performed in the recent past, the work of Lamnaouer, et al. [24] gives insight into the nature of temperature and pressure fields behind reflected shock waves when bifurcations are present. However, as with all simulations, experiments must confirm the behavior modeled by CFD. The authors in [24] give insight into the flow behind the reflected-shock bifurcation in a shock-tube experiment. As observed from the color schlieren images in [19], all features of the bifurcation were seen in simulations done by Lamnaouer et al. in [24]. These include features such as the bifurcated foot of the reflected shock, the separation bubble from the boundary layer under the oblique shocks, and critical to the understanding of hotspots, swirling fluid of the shear layer and wall jet. Lamnaouer et al. also showed the presence of local hotspots in the wall jet after the passage of the bifurcation. Further simulations, such as [25], give evidence for hotspots in bifurcated flows. Combined with experimental schlieren results that indicate early ignition due to hotspots near the shock-tube walls, the numerical results of [25] and [24] give depth of understanding in determining the mechanism for this auto-ignition behavior. Figure 8 shows an experimental example from [25] of auto-ignition occurring in a bifurcated shock-tube flow.

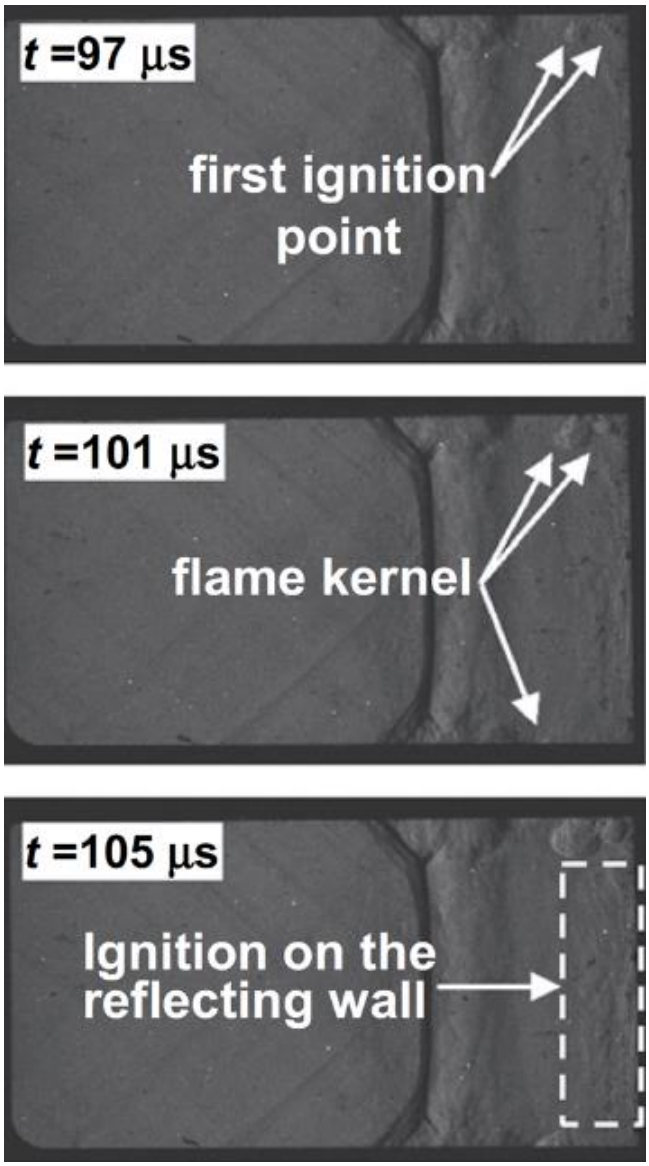

Figure 8. Local ignition behind reflected shock waves with bifurcation. Ignition along sidewall is evident from these schlieren images. Non-dilute C_2H_2-O_2 mixture at 1031 K, 1 atm. Taken directly from [25] with copyright permission from Elsevier B.V.

Other Potential Effects

In any non-dilute shock-tube experiment, bifurcation itself can be a problem. However, non-dilute mixtures cause other issues in shock-tube flow that make data acquisition difficult. As investigated in [14, 15, 26], the reflected shock interaction with

the contact surface will result in driver gas bleeding through the bifurcation. This most assuredly can affect the experimental results. Though this is a realistic concern for shock-tunnel flows, the time scales required for such mixing of the driver gas are much longer than the test times for these methane-based mixtures. Additionally, the curling up of the boundary layer in the separation bubble prevents the cold driver gas from entering the wall jet for some time until after the contact surface interacts with the reflected shock and the test has ended. Thus, driver-gas contamination is not of great concern in the present investigation.

Furthermore, interaction between the reflected shock wave and the contact surface may be of concern should this interaction occur prior to the arrival of the expansion head. Either a compression or expansion wave can reflect toward the endwall as a result of the reflected shock wave interacting with the contact surface, which prematurely ends the test. This gas dynamic phenomenon is shown conceptually in Figure 9. Thirdly, since CO_2 has a higher value of specific heat capacity than N_2, an additional thermal effect will occur in reacting flows with high amounts of CO_2. Because of the better heat-sink capacity of the gas, higher values of C_p will cause the ignition-induced rise in post-reflected-shock conditions (especially pressure) to be less noticeable than in mixtures using pure air, ensuring that interpretation of ignition delay time will be more difficult. In summary, the effect of CO_2 regarding bifurcation in shock tubes is not a trivial one.

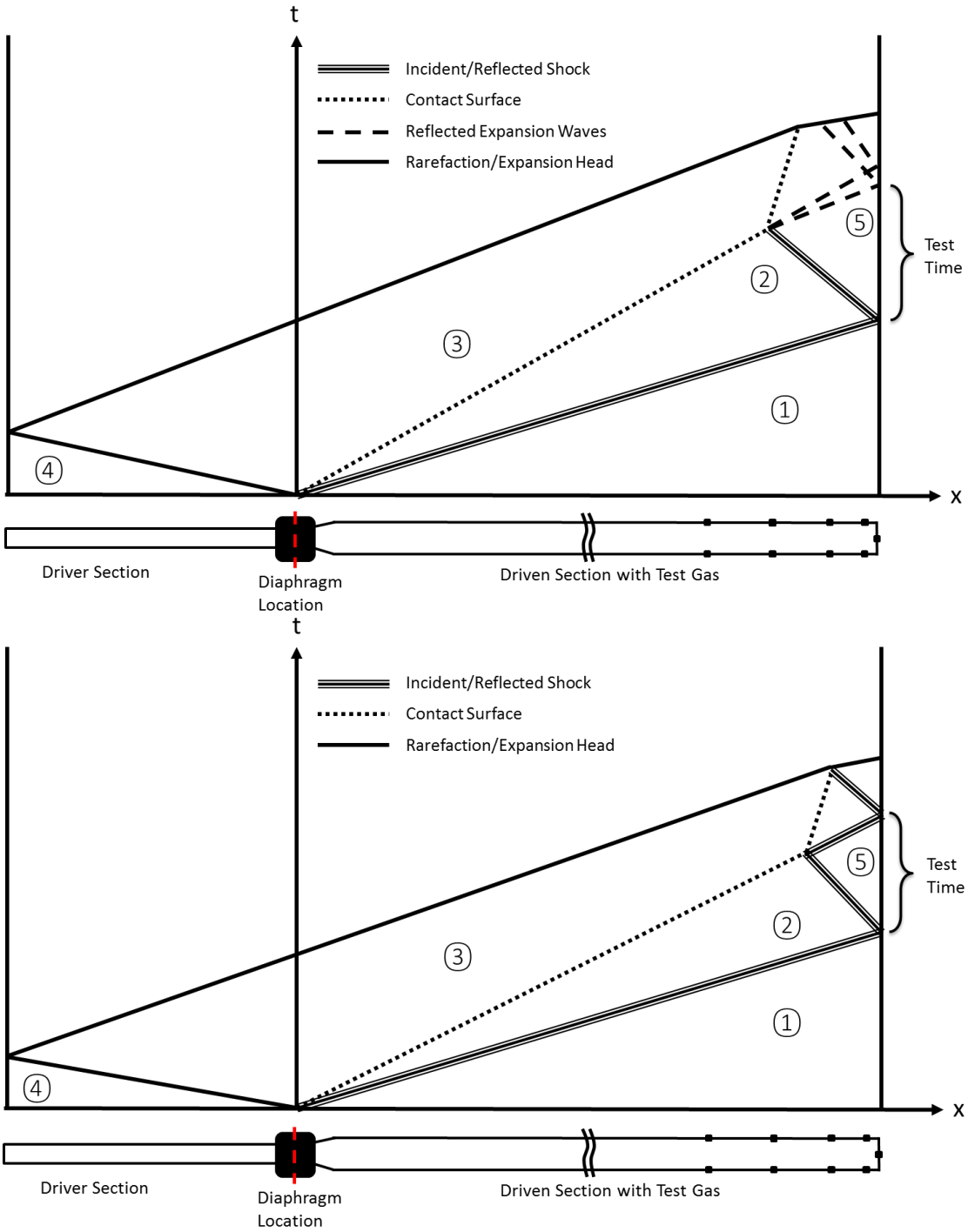

Figure 9. x-t diagram schematics of contact surface interaction with the reflected shock wave in a shock-tube experiment. a) Reflected expansion. b) Reflected compression.

While the bifurcation itself is not of primary concern in non-dilute mixtures when an endwall pressure transducer is used to define time zero, the resulting induced velocity and hot spots in the flow are of great concern. The fluid motion introduced by the second oblique shock wave results in non-quiescent conditions behind the reflected shock, and hot spots introduce areas of non-uniform temperature, pressure, and mixture composition. Conditions such as these are most definitely non-ideal, but seem to be confined to regions near the sidewall of the tube (as shown in the literature from simulations and schlieren imaging). With large-diameter shock tubes, like the ones used in this study, the bulk of the post-reflected-shock flow is assumed to be nearly quiescent and have little variation in temperature, pressure, and mixture composition. Such effects are also minimized when the ignition occurs first and nearly homogeneously at the endwall, where the conditions are most uniform and well known.

Since the presence of diatomic and polyatomic molecules in shock tubes introduces many non-idealities into the flow field, this behavior (though varied) is not unique to one particular diatomic or polyatomic bath gas. Thus, a wide variety of gases can have a similar effect relating to reflected-shock bifurcation, based almost solely on the gas mixtures specific heat ratio [10]. However, the chemical effects during a reaction may vary greatly depending upon bath-gas composition. To explore the chemical effects of CO_2 as a bath gas, a brief investigation into the literature relating to kinetic effects of CO_2 in combustible mixtures was helpful to predict any experimental difficulties outside of the aforementioned flow effects.

Brief Literature Review on Kinetic Effects of CO_2

Multiple researchers have explored the kinetic effect of CO_2 dilution on methane combustion, though few have explored any kinetic effects associated with ignition delay times in shock tubes. A majority of the combustion-related studies reviewed by the author were either conducted in a flame speed vessel or a flow reactor. In [27], both kinetic and thermal effects were observed in the measurement of a premixed flame containing CH_4. Similar effects were observed in [28], [29], and [30]. While [30] was not an experimental study, but a numerical one, it revealed the same conclusions discussed in the experimental studies. In all the studies, it was observed that the primary kinetic effect of CO_2 on the oxidation of methane was through the sub-reaction

$$CO + OH \leftrightarrow CO_2 + H$$

This reaction (in reverse) was observed to have consumed more of the H radicals, which primarily affected the sub-reactions

$$H + O_2 \leftrightarrow O + OH$$

$$CH_4 + H \leftrightarrow CH_3 + H_2$$

by stealing H atoms, allowing less formation of O and OH radicals.

The remaining studies examined the kinetic effect, if any, of CO_2 addition in hydrocarbon mixtures for experiments conducted in shock tubes. Both [31] and [32] investigated the effect of EGR-type mixtures in shock tubes by including CO_2 and H_2O. In both cases, the experimenters saw little to no kinetic effect of CO_2 on the oxidation of methane in lean fuel-oxidizer mixtures other than its behavior as a diluent. This result leads the author to believe that CO_2 behaves primarily as a third body in chemical

reactions; however, the levels of CO_2 addition in these previous works were only on the order of 5% by volume of the overall mixture. Numerical investigations into the third-body effects of CO_2 can be done using a commercially available chemical kinetics solver such as CHEMKIN [33]. An investigation was subsequently performed by the author and is discussed in the results section of this thesis.

CHAPTER IV

RESULTS AND CONSEQUENCES OF HIGH CO_2 CONCENTRATIONS

The experimental results of this study are presented in this section. As recorded previously by Petersen and Hanson [10], bifurcation was expected to be affected primarily by gas composition, and hardly at all by reflected-shock pressure, P_5. Additionally, fluctuations in pressure traces from fluid motion were also expected, and this was indeed the case. Bifurcation was an issue, but other effects of high-CO_2 concentration were observed as well.

Bifurcation

Before the bifurcation results are discussed in full, it should be noted that measurements along the sidewall were not the primary concern in these experiments. If the intent were to have CO_2 as a diluent, and not a replacement for nitrogen in a pseudo-air mixture, sidewall measurements would be necessary to determine the true time zero. In those types of experiments, the true time zero should be determined by use of a laser to detect the passage of the normal portion of the shock wave as in [10]. An endwall transducer is also a good tool to have because fluid motion underneath the bifurcation will surely cause the sidewall transducer to have suspect readings. The experiments for this study, on the other hand, were not conducted in a dilute environment, but one using realistic (and highly exaggerated) EGR mixtures (Tables 1 and 2). Although one does not have to rely on sidewall pressure measurements in flows with high shock bifurcation,

the presence of the bifurcation will surely have an effect on the overall flow conditions behind the reflected shock wave, hence leading to increased uncertainty in the experimental test conditions (i.e., T and P behind the reflected shock wave).

Bifurcation Lengths as a Function of Mixture Composition

While Petersen and Hanson did not investigate reflected-shock pressures below about 10 atm in their work [10], the length of bifurcations in this study still depended strongly on the mixture value of specific heat ratio, γ, agreeing well with their results. As shown in Figure 7, the time from arrival of the bifurcated foot to the time of the pressure overshoot from the stagnation streamline is referred to as Δt_{PO} (following the nomenclature of Petersen and Hanson). Additionally, Petersen and Hanson measured the time from beginning to end of the bifurcation disturbance, Δt_{EO}. Because of the unsteady nature of many of the pressure traces, this time was not easily observed in all mixtures, so only Δt_{PO} is discussed here. The intent of such a comparison is to gauge the relative severity or size of the bifurcation feature. An example trace from this study that more clearly shows this definition is given in Figure 10**.**

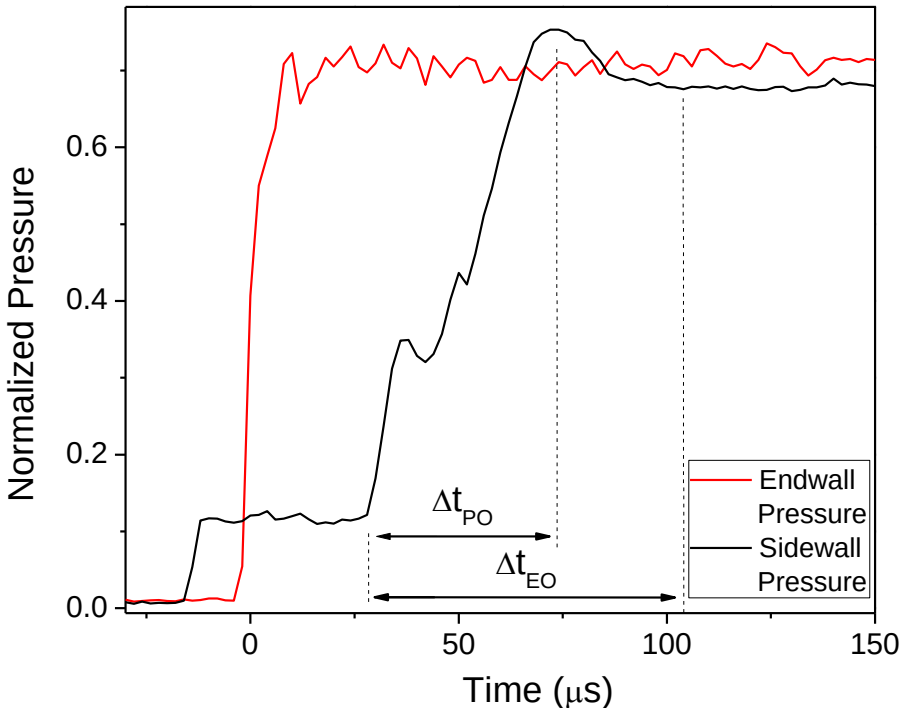

Figure 10. Pressure traces showing time zero defined from the endwall and bifurcation passage over sidewall pressure transducer to define the length of a bifurcation.

Upon examination of the data, the effect of mixture γ was obvious. At pressures near 1 atm in the AST, bifurcation lengths strongly depended upon mixture composition. Mixtures with high levels of CO_2 had larger levels of bifurcation, as expected. Figure 11 shows an example of bifurcation variation over the four different mixtures as seen by the sidewall pressure transducer. It is important to note that while the traces may not be perfectly smooth (as is the nature of sidewall pressure traces with bifurcation), the increasing Δt_{PO} is readily seen in all mixtures.

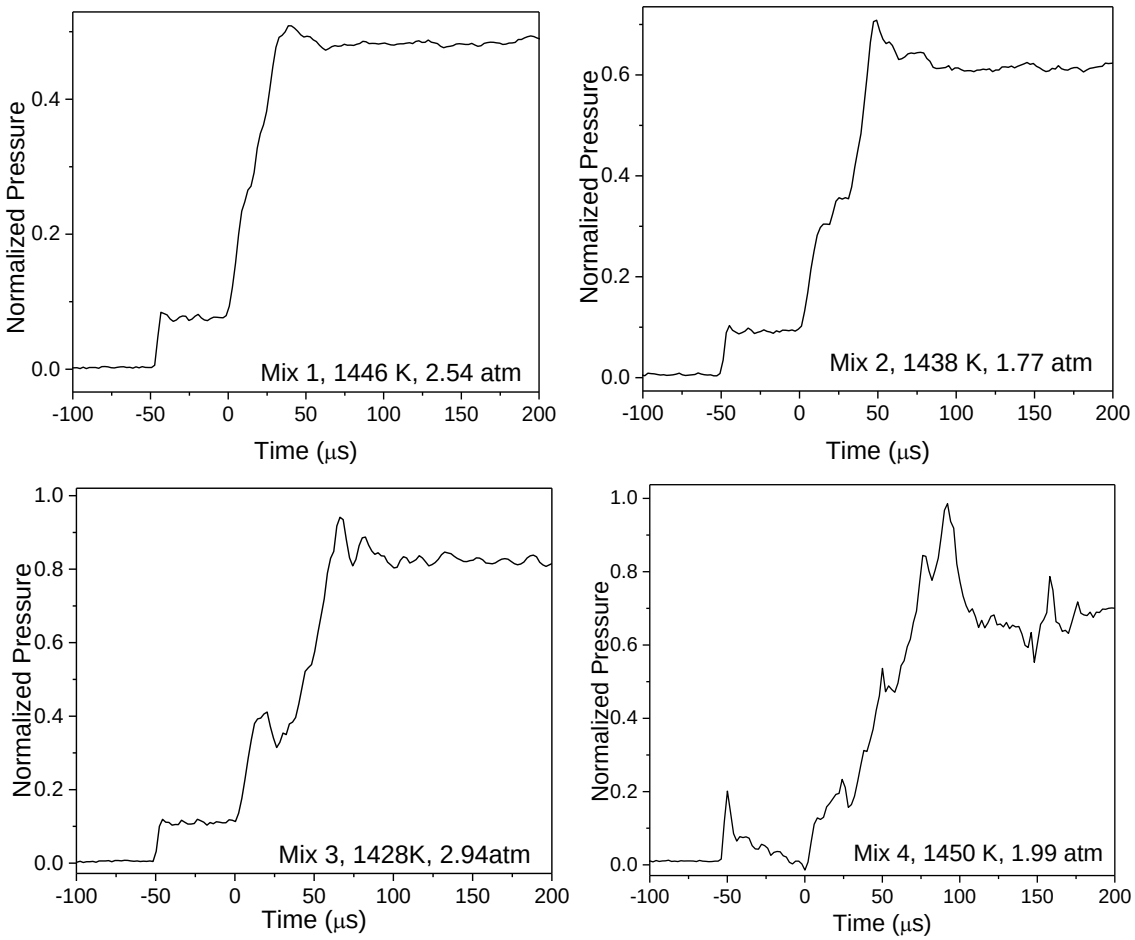

Figure 11. Sidewall pressure traces showing bifurcation behavior at the sidewall pressure transducer for the 4 hot flow mixtures in the AST at low pressures and similar temperature conditions. Note that the traces have been shifted so that the arrival of the bifurcated foot occurs at time zero. Also, these are purely flow effects with no ignition taking place.

To be sure that this trend of longer bifurcations was not limited to a certain T_5 condition, bifurcation lengths (Δt_{PO}) were plotted against T_5 for each mixture.

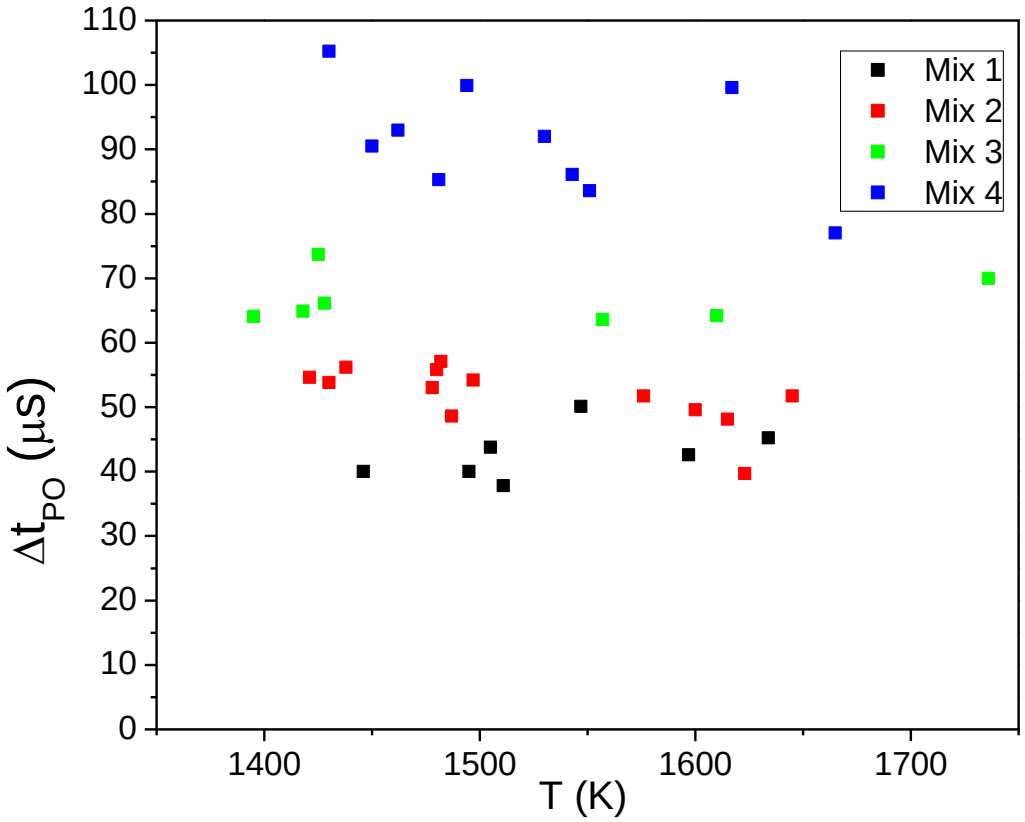

Figure 12. Bifurcation magnitude for each mixture in the AST at low pressures (~1 atm).

From Figure 12, it is seen that bifurcation lengths (or bifurcation times) depend heavily upon mixture composition. The same conclusion can be drawn for experiments conducted in the HPST at pressures near 10 atm. Figure 13 shows the same dependence upon mixture specific heat ratio at the 10-atm pressure range (only Mix 1 and Mix 4 were investigated in the HPST). Figure 14 also shows similar results to those in Figure 12.

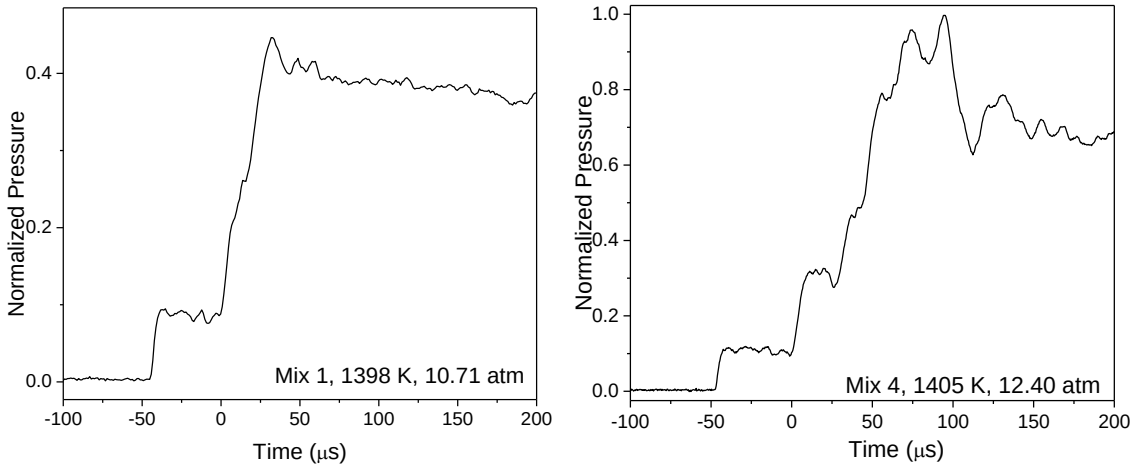

Figure 13. Sidewall pressure traces showing bifurcation behavior at the sidewall pressure transducer for Mix 1 and Mix 4 in the AST at low pressures and similar temperature conditions. Note that the traces have been shifted so that the arrival of the bifurcated foot occurs at time zero. Also, these are purely flow effects with no ignition taking place.

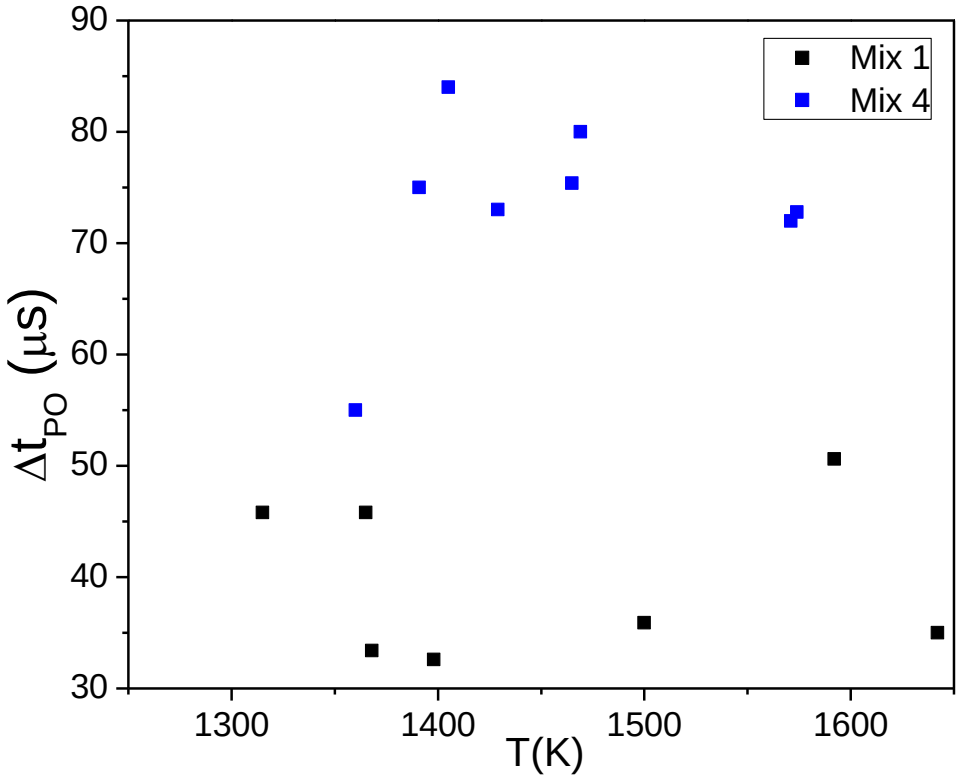

Figure 14. Bifurcation magnitude for Mix 1 and Mix 4 in the HPST at high pressures (~10 atm).

When the data from Figure 14 and Figure 12 are combined, the results show very little dependence on P_5, as seen also in Petersen and Hanson [10]. Note also that there is no dependence of the bifurcation magnitude on T_5 (i.e., shock speed) as well.

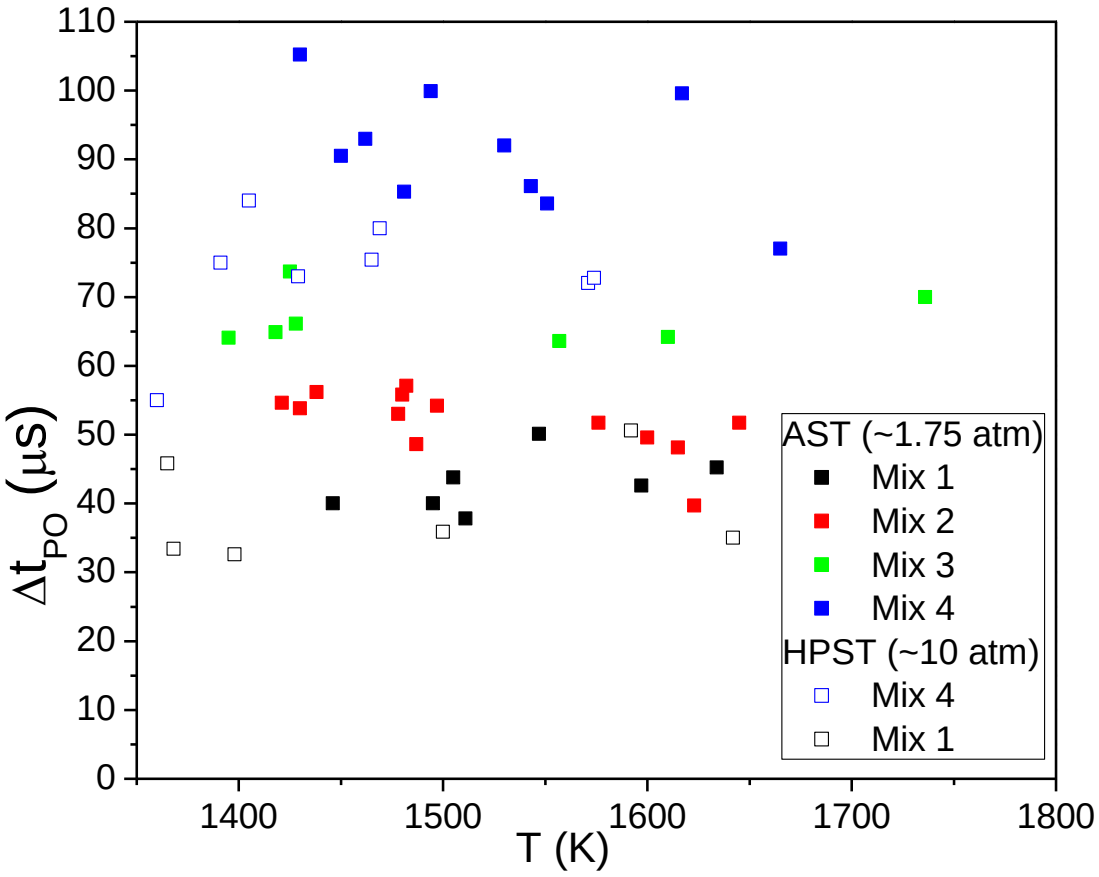

Figure 15. Bifurcation magnitude in terms of time span for all hot flow mixtures in both the AST and HPST.

Though the data show distinctions between each mixture, the data for Mix 4 do seem to differ slightly between 1 and 10 atm. A potential explanation for this difference comes from boundary layers behind the incident shock. Since the boundary layers for the high-pressure shocks ($P_5 \approx 10$) are most likely turbulent almost at inception due to the higher Reynolds number, each of the experiments conducted by Petersen and Hanson in [10] were likely conducted where the reflected shock propagated back into an oncoming turbulent boundary layer. In the lower-pressure experiments conducted in the AST, however, the boundary layers could have been laminar rather than turbulent. Since laminar boundary layer thicknesses have a more distinct pressure dependence compared with those in turbulent flow, reflected-shock bifurcation behavior would also be affected. Lower pressures with thicker boundary layers can cause the bifurcation to grow more quickly, giving higher values of Δt_{PO} for the low-pressure experiments. It should be noted that though the two tubes had differing lengths, values of T_5 and incident-shock Mach number (as well as composition) were nearly the same at the time of shock reflection during each experiment. More investigation into discernment of laminar versus turbulent boundary layers is discussed in the next chapter.

Pressure Noise from Fluid Motion

Because bifurcations not only mask the arrival of the reflected shock wave, but also create eddies and a vortex sheet, they generate much fluid motion in the form of vorticity. This fluid motion was observed in the form of pressure oscillations near both the sidewall and endwall pressure transducers. Just like how the bifurcation lengths varied with mixture composition, the scale of pressure oscillations were also observed to

vary with mixture composition. Figure 16 shows greater pressure oscillations in both the sidewall and endwall pressure traces with increasing amounts of CO_2. The increase in pressure oscillations is gradual between the traces from Mix 1 and Mix 2, and similarly from Mix 2 to Mix 3. But when the traces of Mix 4 are examined, the pressure oscillations are more readily evident. Also, the sidewall pressure traces seem to show a clearer gradient from less fluid motion to more fluid motion from vorticity ranging from Mix 1 to Mix 4. Since the bifurcations are larger with more CO_2, more large-scale fluid motion is generated. These high vorticity regions pass directly over the sidewall pressure transducers, so they show up in the pressure traces more readily. Also, since the endwall port does not observe the fluid motion from the vortex sheet until the vortices curl up the endwall of the tube, the pressure oscillations are not observed as easily when bifurcations are less severe. The bifurcations in Mix 4, however, seem to be quite severe and induce significant vorticity near both the sidewall and endwall transducers.

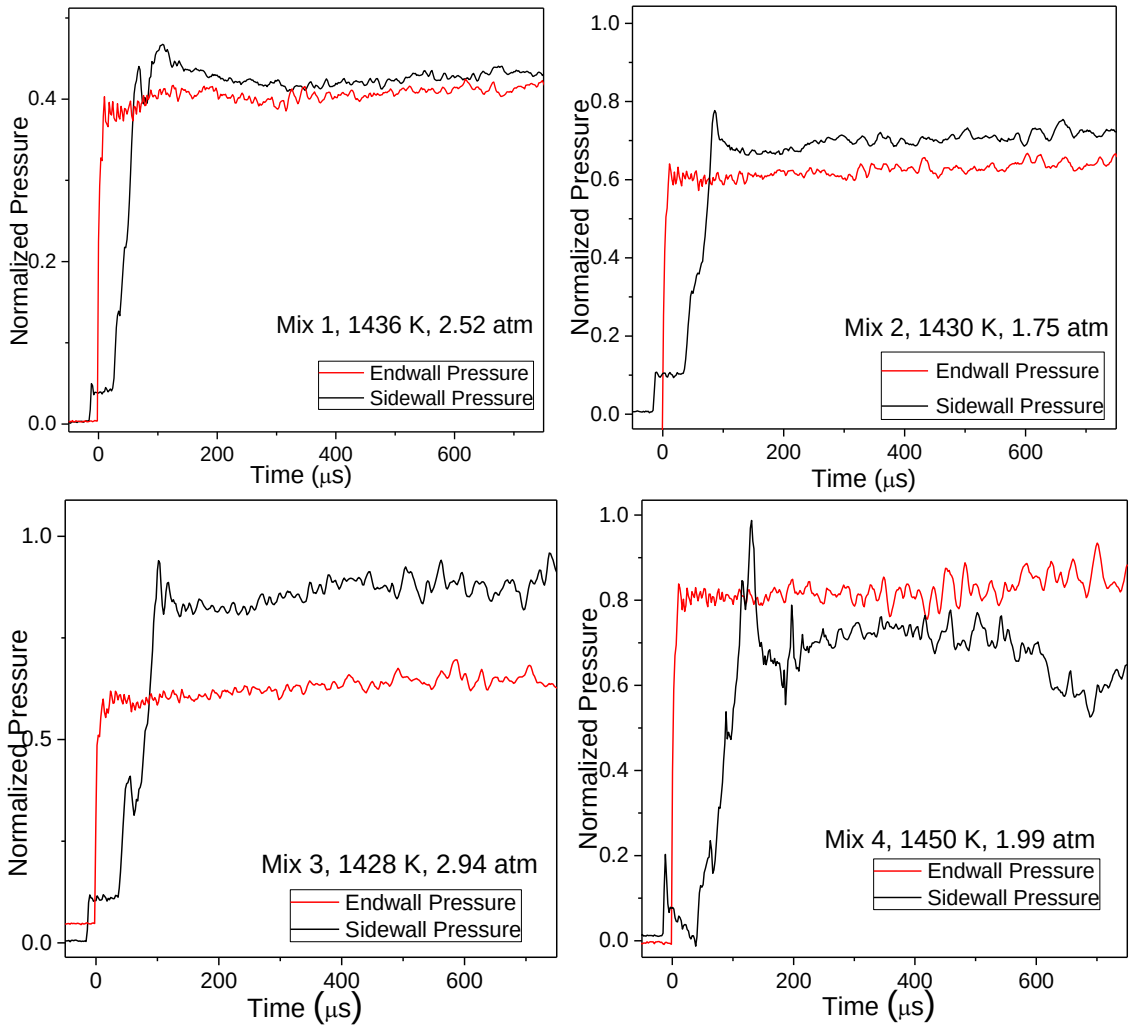

Figure 16. Variation in pressure oscillations as a result of bifurcation for the hot mixtures in the AST at one T_5 condition. These are purely flow effects with no ignition taking place.

To establish a baseline of what features in the pressure traces to expect from the bifurcated runs, the cold flow mixtures were used to verify this messy behavior behind the bifurcations. Such a baseline is important since features in the pressure can occur upon ignition, so one needs to be able to distinguish such differences between features

due to the bifurcation event. Figure 17 confirms increased vorticity in the high CO_2-content mixtures. Fluid motion was more distinct as CO_2 content was increased.

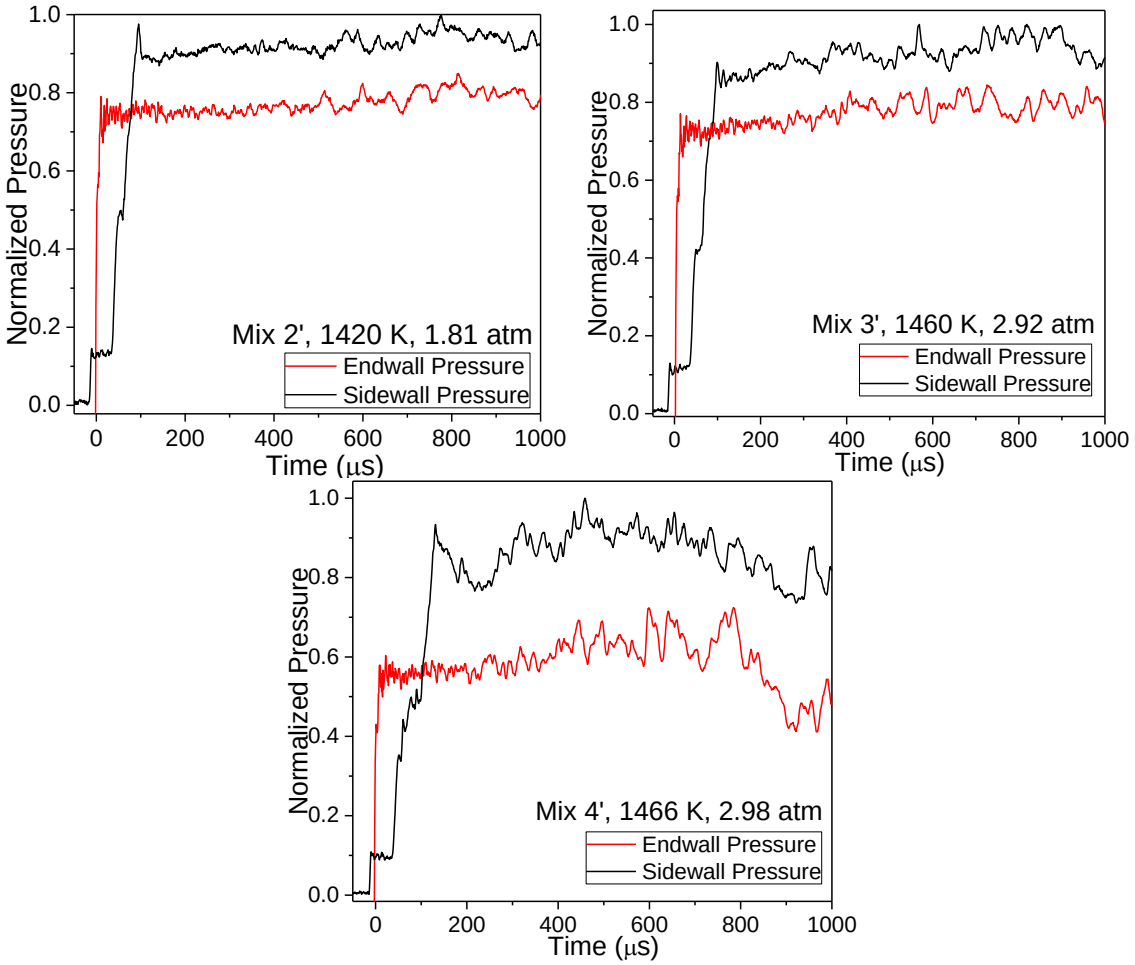

Figure 17. Variation in pressure oscillations as a result of bifurcation for the cold mixtures (2'-4') in the AST.

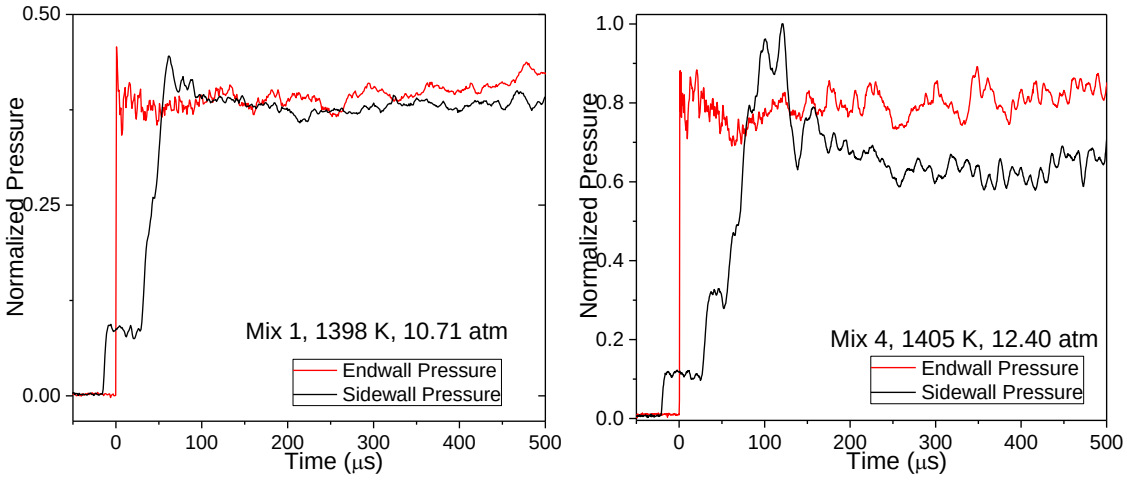

Figure 18. Variation in pressure noise as a result of bifurcation for Mix 1 and 4 in the HPST. These features are purely flow effects with no ignition taking place.

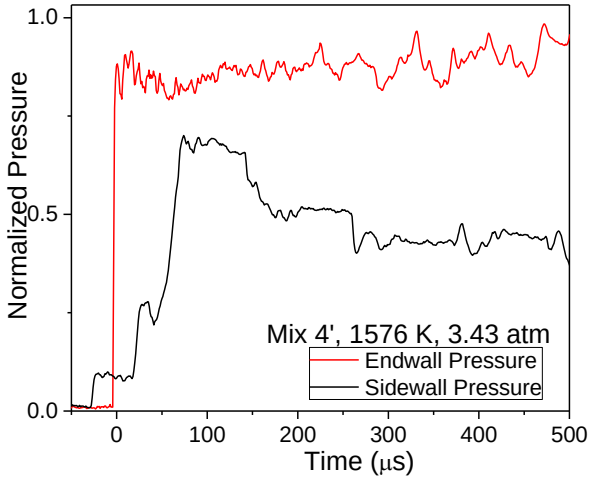

Figure 19. Variation in pressure noise as a result of bifurcation for cold mixture in the HPST.

Decreased Energy Release

Along with the effects of bifurcation, mixtures with high levels of CO_2 proved more difficult to analyze due to suppressed ignition. With added CO_2, the mixtures had a higher overall value of specific heat capacity, C_p. Though the post-reflected shock conditions were nearly the same for Mix 1 compared to Mix 4, the observable energy release (in the form of a pressure spike) was lower. Figure 20 shows time histories for the 4 different mixtures near a common temperature. While the pressure spikes from ignition in Mix 1 and Mix 2 may look similar, Mix 3 has less of a P-rise than the first two mixtures, and Mix 4 has the smallest relative pressure rise of all the mixtures.

At this juncture, a brief aside is necessary. For mixtures with CO_2 (especially Mix 4), the sidewall pressure and emission traces were of little use in characterizing ignition behavior due to the fluid motion associated with reflected-shock bifurcations. Also, as was discussed in [8], non-dilute fuel-air mixtures are best observed using endwall diagnostics since the high-enthalpy flows can cause the sidewall locations to predict ignition that appears to be earlier than at the endwall. That is, in such mixtures the ignition event at the endwall is very strong, leading to an explosion wave that appears to occur within the entire endwall region more or less at once. The end result is that the ignition delay time from a sidewall location (where its time zero is different from the endwall's time zero) is shorter when compared to the true ignition delay time relative to the endwall.

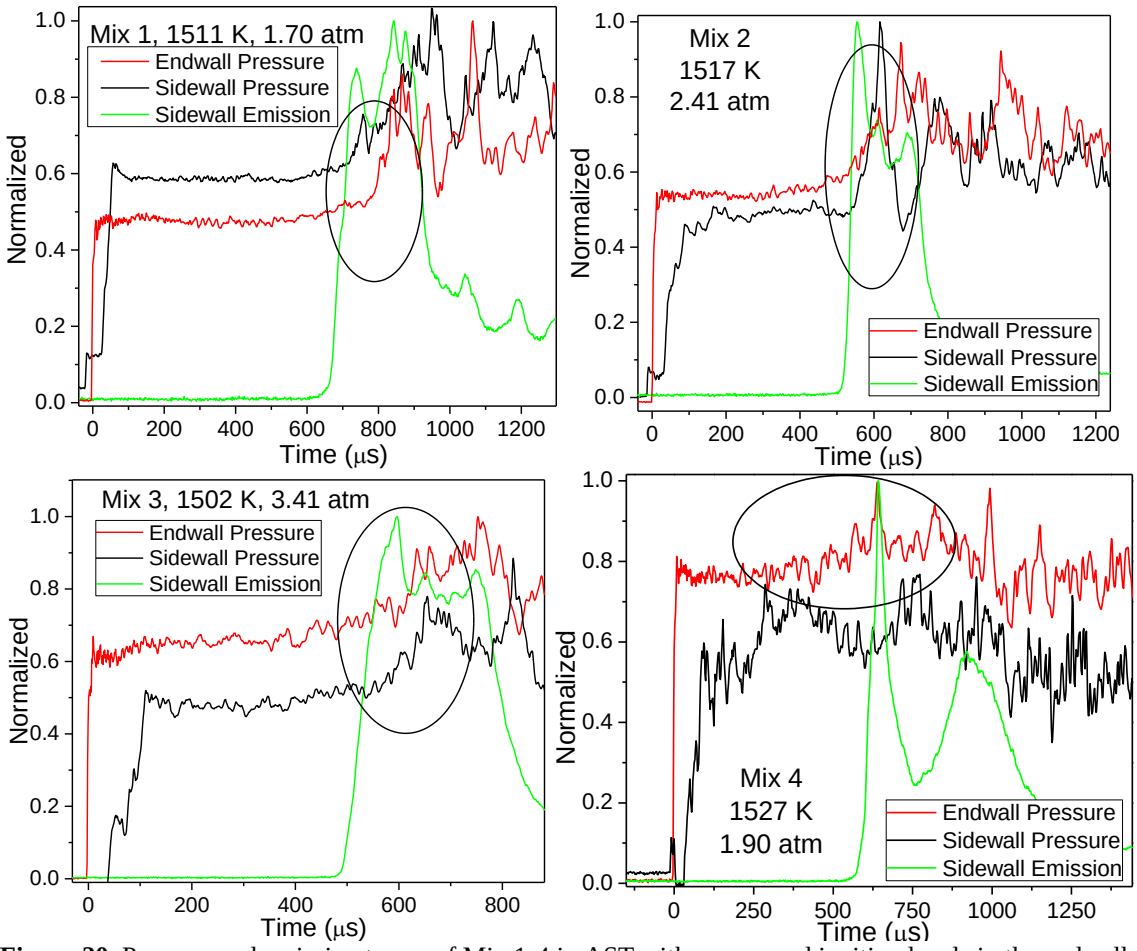

Figure 20. Pressure and emission traces of Mix 1-4 in AST with suppressed ignition levels in the endwall pressure trace. The endwall pressure transducer is the primary ignition diagnostic in these traces. Ignition regions are circled.

Other behavior such as early, non-homogeneous ignition due to hotspots can be detected at the sidewall ports, so it is also useful to monitor sidewall traces for such behavior. Early ignition time from a sidewall port (but in relation to time zero defined at the endwall) is an indicator of hotspots within the flow. Were uniform ignition truly occurring in these types of experiments, it would occur first in a region near the endwall. Hotspots near the sidewall can cause auto-ignition and the formation of spherical

combustion waves that tend to be observed by sidewall ports before endwall ports (from transducers and/or optical emission/absorption). Figure 8 shows an example of this occurring in an experiment with acetylene. Thus, the sidewall pressure and emission traces are shown hereafter not as an exact indicator of ignition times, but as a general guide as to when the main ignition event was occurring. Since the AST did not have an emission diagnostic at the endwall, and the pressure traces had much noise, etc., sidewall measurement of OH* emission was helpful in showing that an ignition event had occurred in the shock tube.

Since the effect of suppressed ignition is primarily a thermal effect, determining such effects numerically is a straightforward process. In fact, a quick hand calculation for adiabatic flame temperature (at constant-internal energy, constant-volume conditions) would reveal a higher temperature for Mix 1 than for Mix 4. CHEMKIN [33] can also predict the pressure and temperature rise due to ignition. Figure 21 shows temperature and pressure versus time for Mix 1 and Mix 4 during the process of ignition. It can be concluded from Fig. 21 that the higher CO_2-content mixtures have a more subdued ignition event.

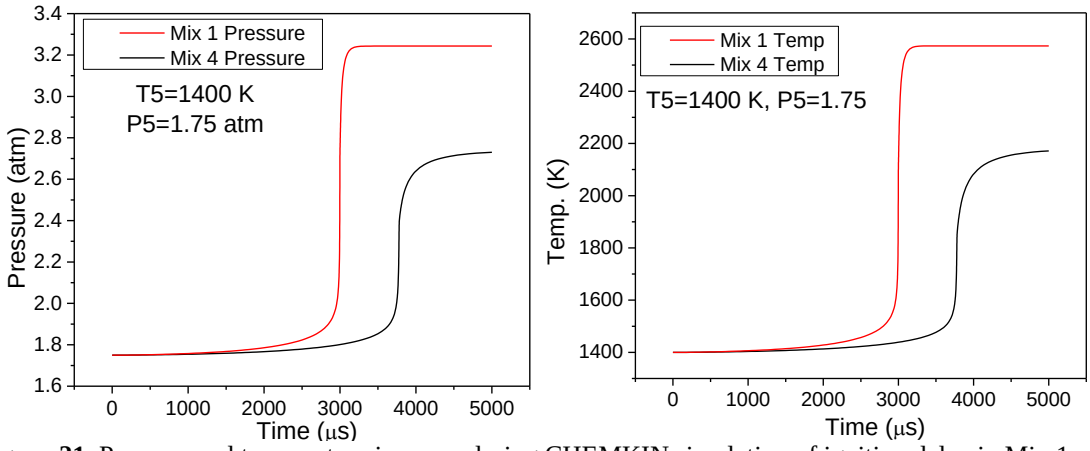

Figure 21. Pressure and temperature increase during CHEMKIN simulation of ignition delay in Mix 1 and Mix 4.

Though all the difficulties discussed so far have inhibited the interpretation of the data to a certain extent, none of them invalidated the data. The next problem associated with these non-dilute mixtures caused some of the data to be completely unusable.

Pressure Discontinuities

Up to this point in the results concerning effects of CO_2 in non-dilute shock-tube experiments, all the effects have been hindrances to reading the data, but none have made data from any given experiment completely unusable. While pressure oscillations existed in all of the experiments, none of the non-idealities discussed thus far have caused a sudden drop-off or shift in reflected-shock conditions. However, such problems existed when examining several of the lower-temperature experiments. When ignition did not occur within a certain time frame (differing slightly for each mixture), a sharp pressure drop-off or jump would be seen in both the sidewall and endwall pressure traces. In shock-tube experiments, such pressure changes are tied to temperature

changes. At present, it is not clear what the exact cause of these pressure discontinuities is, but they are almost certainly due to an expansion process. The observed behavior, though, does seem to align with that of the interaction of the reflected shock wave with the contact surface (or contact region) between the driver and driven gases created after the rupture of the diaphragm. This possibility is discussed more in the next chapter. Figure 22 shows examples of the pressure drop-offs for the different Mix 1-4 in the AST at a given temperature condition. Upon examination, the time histories show that the pressure drop-offs begin at approximately the same time, but the rate of the change is greater for mixtures with higher amounts of CO_2.

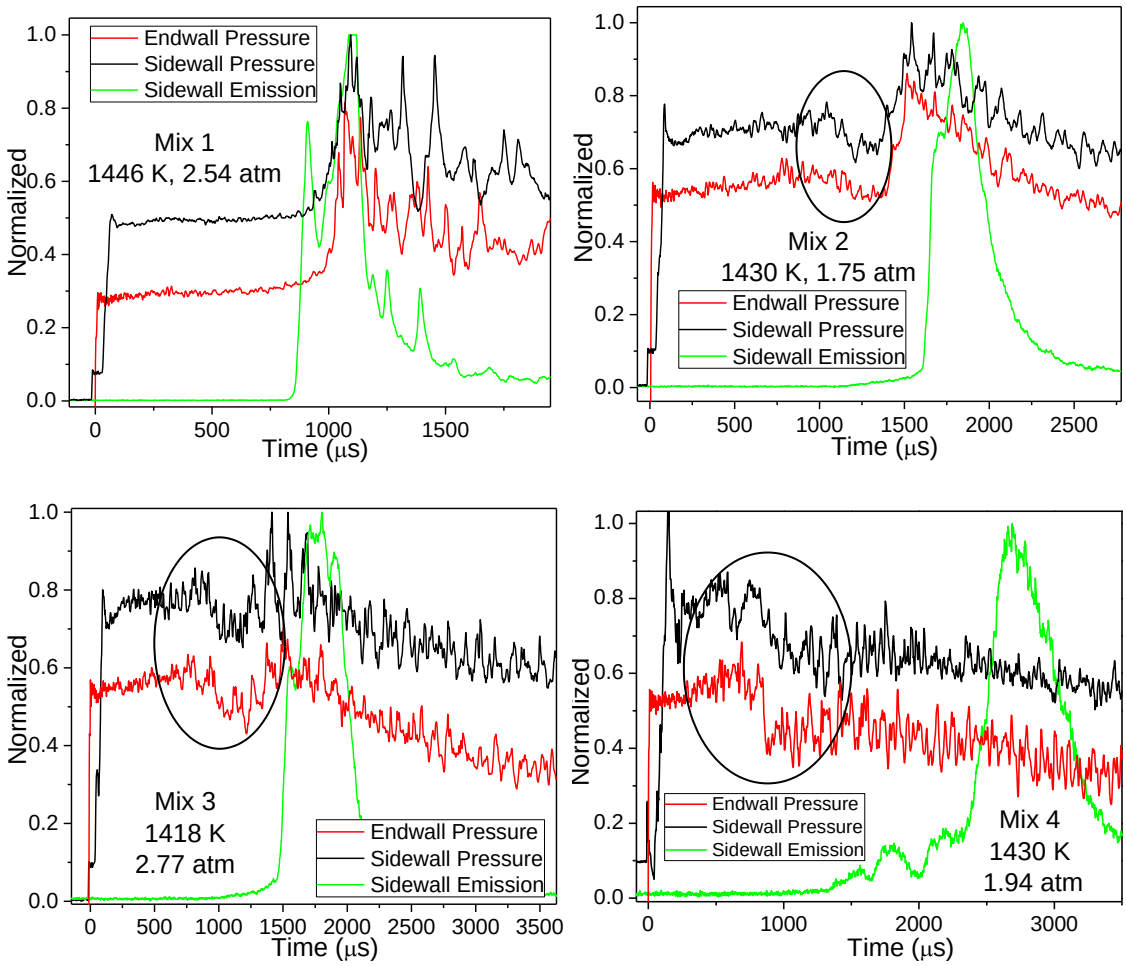

Figure 22. Pressure and emission traces from hot-flow experiments showing the pressure expansion behavior (in circles). The endwall pressure data in the graphs have been shifted down to give a clearer view of the traces.

As was done before, the hot-flow mixtures in the AST were mimicked by cold-flow mixtures with equivalent values of specific heat ratio. Figure 23 shows similar behavior to the hot-flow mixtures in Figure 22. Thus, it can be concluded that this phenomenon is not attributed to reactivity of the mixture, or to any unseen chemical

reactions, but is by nature a fluid-mechanic flow effect. The same phenomenon was seen in the HPST for Mix 4 and Mix 4' but not in Mix 1, shown in Figure 24 and Figure 25.

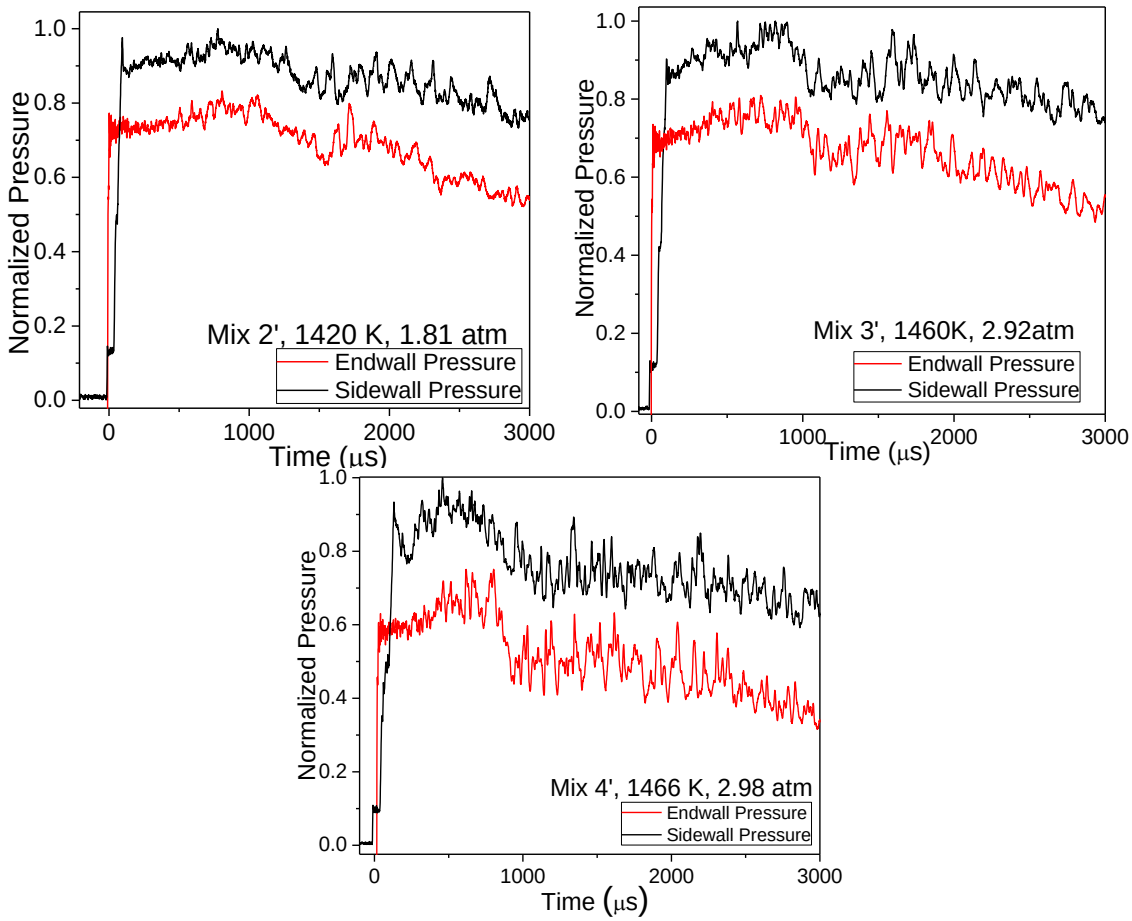

Figure 23. Cold flow for Mix 2'-4' in the AST. The pressure discontinuity grows more noticeable with increasing CO_2 content. As in Figure 22, the endwall data have been shifted down for easier viewing.

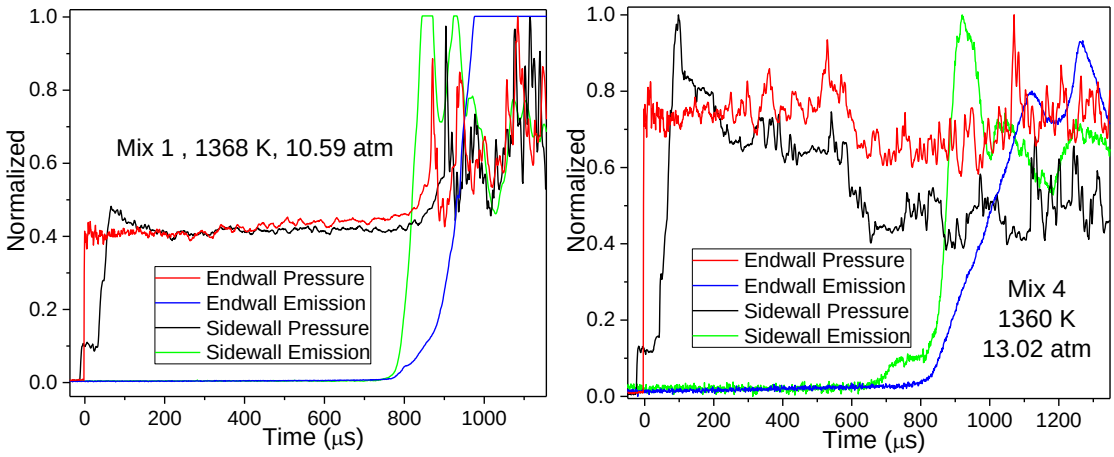

Figure 24. Mix 1 and Mix 4 in the HPST. The pressure drop-off is seen in Mix 4, but not in Mix 1.

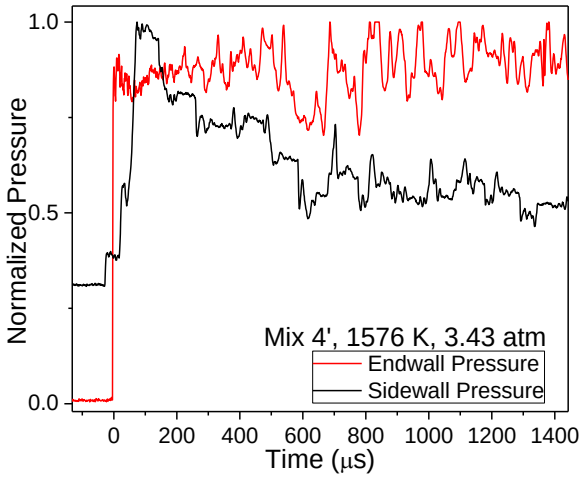

Figure 25. Example of the pressure discontinuity in the HPST for Mix 4' (cold flow).

From the figures shown in this section, the presence of the pressure expansion behavior can be seen, but the mechanism by which it occurs could not be confirmed with only first-order calculations. The observed rate at which the pressure change at this expansion did vary with mixture composition (less severe with less CO_2), but it also changed with incident Mach number and pressure, P_1, which determine T_5. For example,

examine the plot of Mix 2' in the AST in Figure 23. The pressure drop-off is very small at 1420 K. Examination of Figure 26, however, reveals a very different behavior. A pressure change still exists, but it is a sharp increase instead of a drop-off. These kinds of behaviors were observed in mixtures where reflected-shock temperatures, T_5, were in the upper end of the investigated temperature range, ~1800 K and above. Evidence of varying pressure interactions (for the same mixture) with differing temperature is what led the author to believe this phenomenon is related to contact-surface interaction.

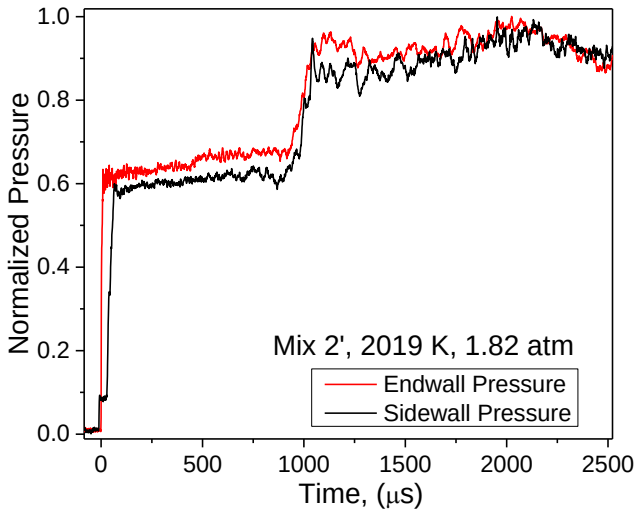

Figure 26. Cold flow in Mix 2', showing a pressure rise at a high T_5 instead of a drop-off like at lower temperatures.

Regardless of the cause of these pressure changes, they effectively end an experiment. While ignition events are still observed after the pressure drop-off, the conditions can no longer be assumed the same as the original T_5 and P_5 at time zero (for cases like Figure 26, ignition occurred before the pressure rise because of high T_5). Thus,

none of the cases where a pressure drop-off occurred prior to ignition can be relied upon to provide an ignition-delay time data point. Despite all the non-idealities, ignition delay time data was collected, and the results differ very little from Mix 1 to Mix 4 at either pressure condition, as discussed next.

Effects on Ignition Delay Time and its Interpretation

As a result of high CO_2 concentration in the EGR-based mixtures, many non-ideal effects were present in the reflected-shock-wave data. For the most part, ignition delay time could still be interpreted from the measured pressure and emission data. With more CO_2, the true time zero (defined from the endwall pressure trace) was not disrupted by bifurcations, but induced fluid motion was more evident and muddied the traces. Additionally, the pressure rise from ignition was harder to detect because of the high specific heat capacity of CO_2 compared to N_2. Lastly, some of the runs were ended prematurely by the arrival of a pressure expansion before the onset of ignition. Overall, these non-idealities prevented a sharp pressure rise during ignition in most of the experiments with CO_2, unlike in Mix 1. Although ignition onset was still apparent, uncertainty was added to its interpretation for the higher-CO_2 mixtures.

Figure 27 gives an example of how ignition delay time was defined in experiments where non-idealities from CO_2 had significant influence. Since the pressure rise at the endwall was not sharp, but smooth, 2 tangent lines were drawn through the data (as is done in dilute experiments using a sidewall emission trace) and their intersection was defined as the point of ignition onset. This ignition point is not without

uncertainty, though, since the un-stationary fluid causes the pressure trace to fluctuate to a greater degree than in a stationary fluid.

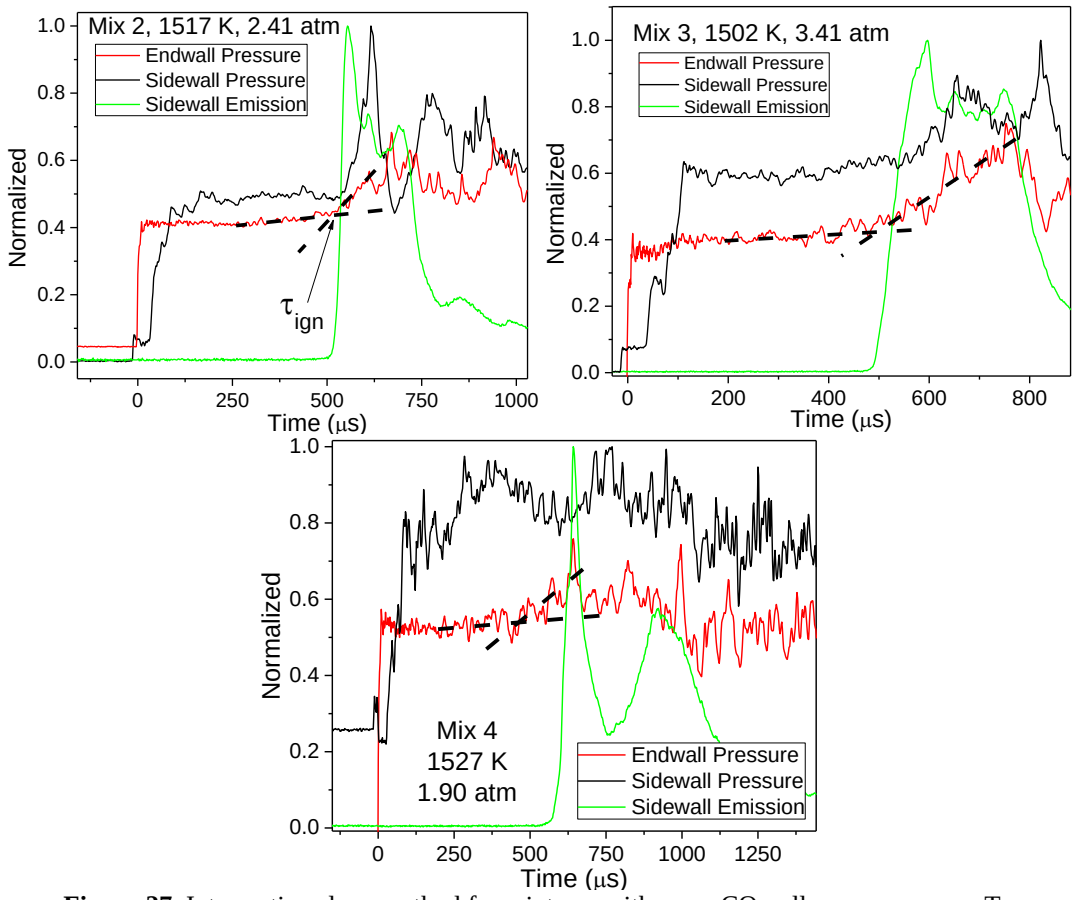

Figure 27. Intersecting slope method for mixtures with more CO_2, all near a common T_5.

Using a pseudo-slope-intersection method is a less-precise way to define ignition delay time in these mixtures, so the determination of the ignition delay time must be interpreted on a case-by-case basis. Figure 28 shows why the intersection of the two lines has an accompanied uncertainty. With the inherent fluctuations in these pressure traces, the initial rise of the pressure trace near the point of intersection may occur just because of circulating fluid, with the true pressure increase occurring shortly after. Thus,

with the uncertainty in the pressure rise due to fluctuation of the trace, the definition of ignition delay time has added uncertainty as well. This uncertainty is greater than any uncertainty in T_5 or P_5 conditions given from the shock-velocity measurements and normal-shock relations. Additionally, the added uncertainty is not easily calculable in an analytical way and was therefore included in more of a brute force manner by including error bars in subsequent ignition delay time plots.

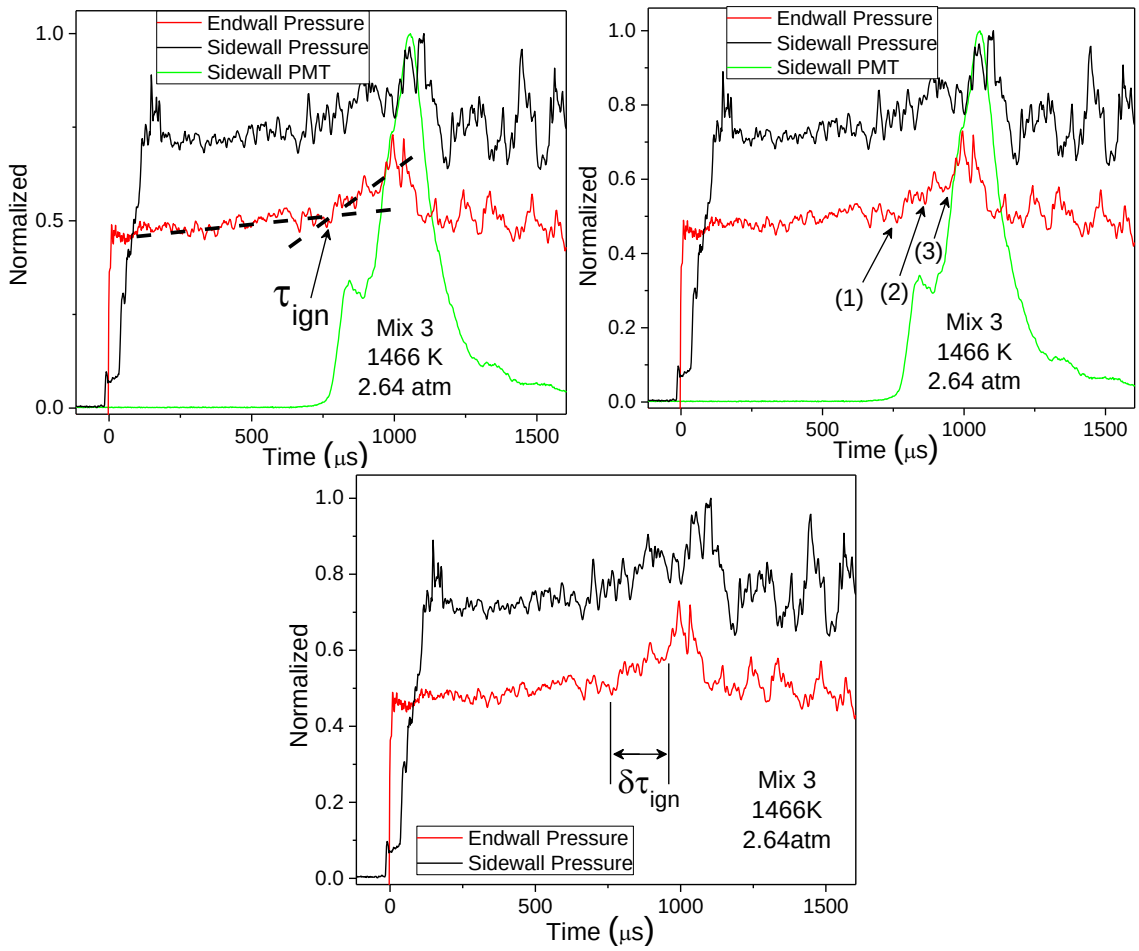

Figure 28. Method for defining ignition delay time in mixtures with noisy pressure traces and suppressed ignition pressure rise. a) Two intersecting slopes define the time of ignition, b) Because of non-quiescent conditions additional uncertainty in ignition time is introduced (shown with three possible times). c) The last figure has no emission to more clearly show the range of uncertainty.

Even though the AST did not have an endwall emission diagnostic, ignition delay times inferred from the pressure transducer located at the endwall were satisfactory. The HPST, as mentioned earlier, was equipped with both emission and pressure diagnostics at the endwall. When considering the HPST results, displayed in Figure 29, the addition of the endwall diagnostic is somewhat helpful in the case of Mix 1, but less so for Mix 4. An endwall emission trace helps to detect any pre-ignition down the length of the shock tube in these high-enthalpy experiments, but gives no added benefit in observing ignition delay times. Similarly, the endwall emission diagnostic could discern pre-ignition in the high-CO_2 mixtures, such as Mix 4. Upon closer examination of the blue endwall emission trace in Figure 29, though, an idea of when ignition occurs can be estimated, but with no greater certainty than the sidewall emission trace. In fact, the sidewall trace may be more helpful in this case since it increases more smoothly and more suddenly than the endwall emission trace.

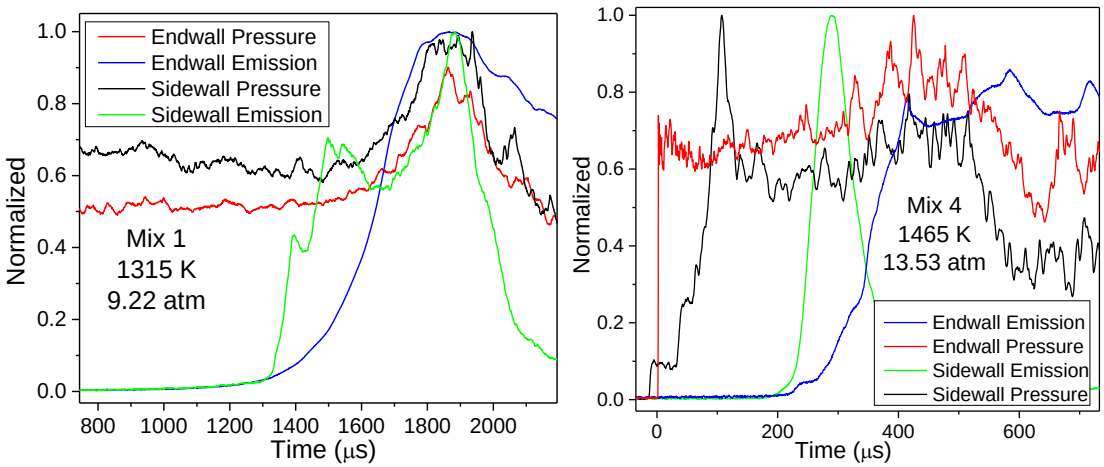

Figure 29. Experiments conducted in the HPST near 10 atm. Even with an endwall diagnostic, interpreting ignition delay is still a challenge in Mix 4.

After examining the data and taking into consideration all non-idealities present, the ignition delay time behavior of all 4 mixtures were very similar. Figure 30 shows the ignition delay times of each mixture over the range of T_5 conditions on an Arrhenius plot. Mix 2-4 are plotted individually compared with Mix 1, each with a model comparison to the Aramco 1.3 mechanism from the National University of Ireland in Galway, Ireland [34]. The agreement between each mixture and the model for that mixture is very good. Also, all of the mixtures behave very similarly, even with the inclusion of uncertainty in ignition delay times in each mixtures. Something to note, the y-axis is plotted on a $\log_{10}$-scale. Thus, the error seems greater for the higher-temperature experiments (smaller values of $10^4/T$), though it is actually much less than for the lower-temperature experiments.

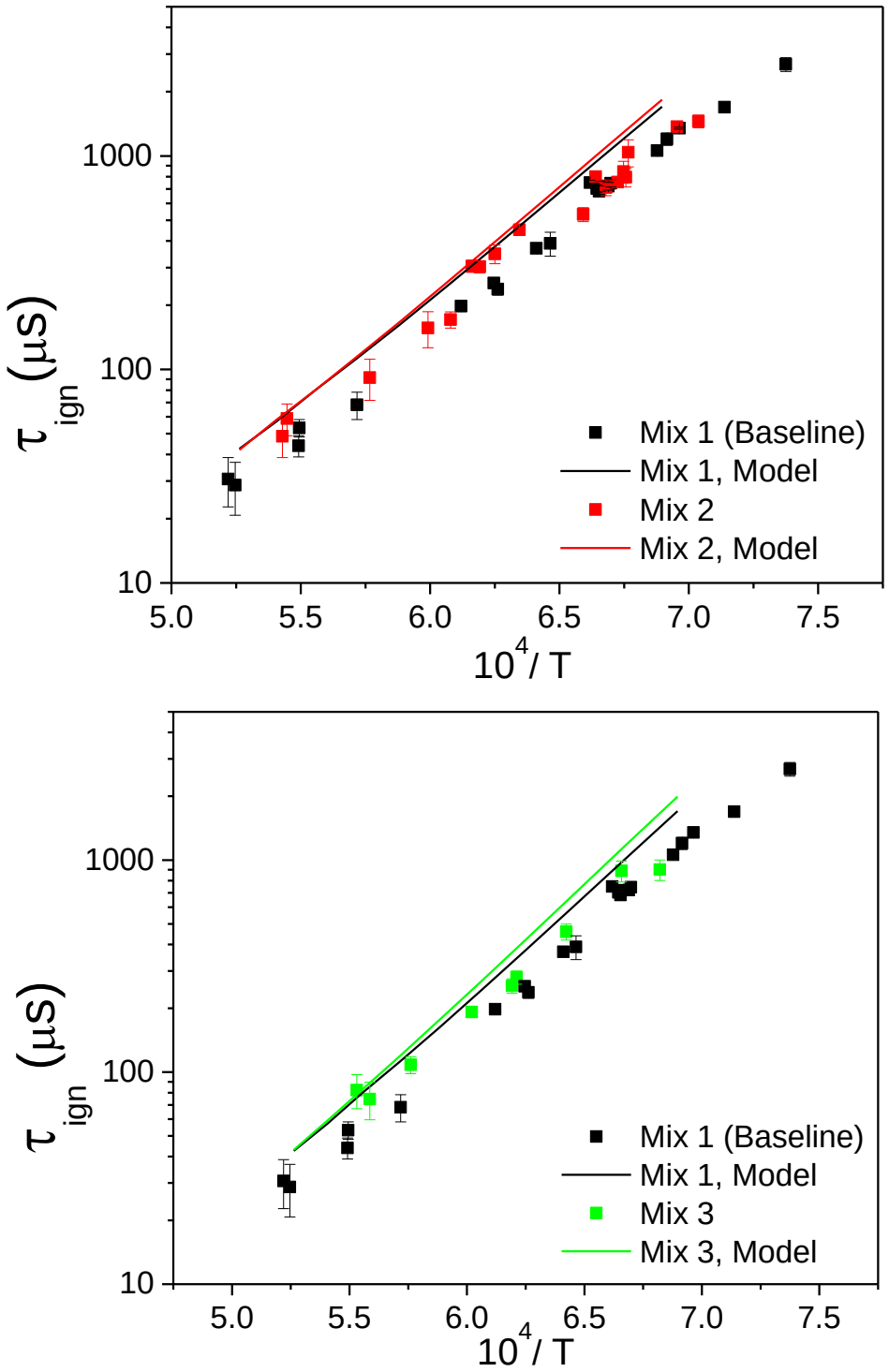

Figure 30. Ignition delay times for each mixture at 1.75 atm, shown compared to Mix 1 on an individual basis, then together. a) Mix 1 vs Mix 2, b) Mix 1 vs Mix 3, c) Mix 1 vs Mix 4, d) All mixtures. The model referred to in the graphs is the Aramco 1.3 mechanism from NUIG.

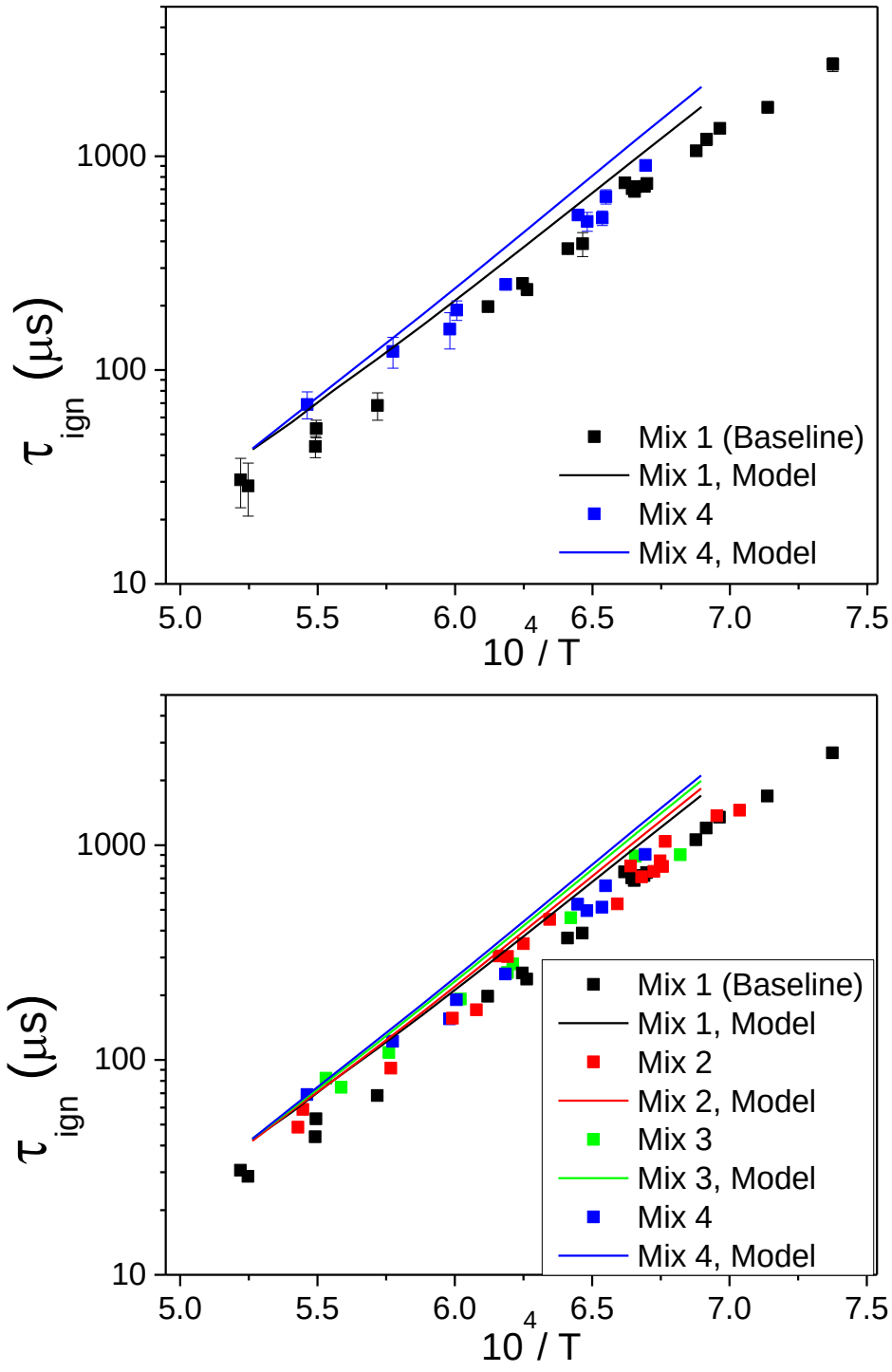

Figure 30. Continued

Similar to the low-pressure ignition delay time results in the AST, the high-pressure experiments in the HPST showed good agreement with the model. Figure 31 shows that for the higher pressures, the uncertainty in ignition delay time is greater. This increased uncertainty makes sense since the higher-pressure experiments are likely to have only turbulent boundary layers, so therefore the bifurcations will also likely have more-turbulent effects in high-pressure situations than in low-pressure situations. Upon comparing Mix 1 and Mix 4 for both the data and the model, though, it seems that CO_2 has a slight effect on ignition delay time when comparing mixtures 1 and 4, respectively. Figure 31 shows that when CO_2 is a major component of methane mixtures near pressures of 10 atm, ignition delay times are longer than in mixtures without CO_2.

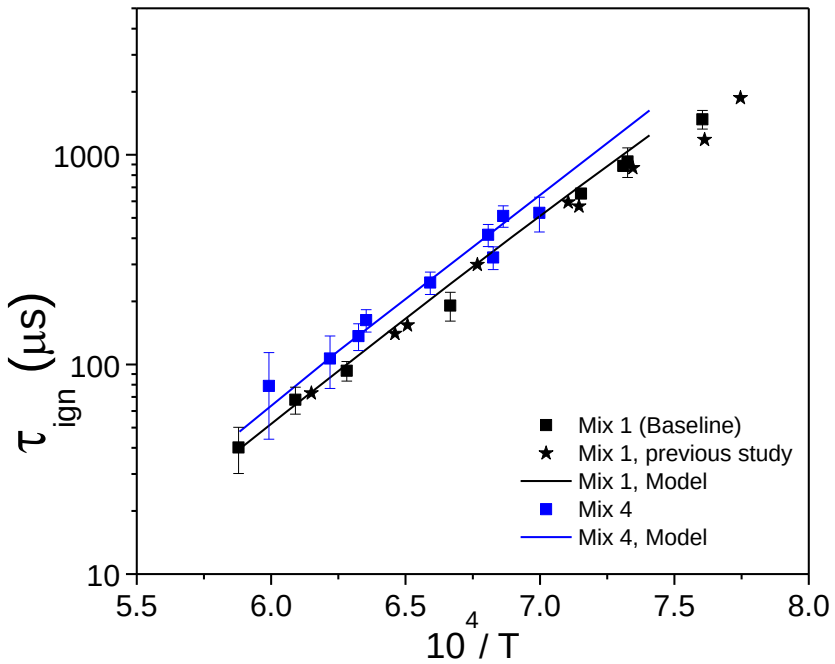

Figure 31. Ignition delay times for experiments in the HPST at 10 atm.

Previously, it was shown that if a pressure drop-off occurred during an experiment, that experiment was effectively over and its data discarded. This rule was the assumption in the ignition delay time plots from Figure 30. Interestingly, upon including ignition delay time data from experiments where a pressure drop-off occurred, the observed behavior of these experiments still fit reasonably well for both the AST and HPST data at low and high pressures, respectively. Figure 32 includes the extra data from the AST experiments as open boxes. The formerly discarded data are well within the scatter of the original data for all the mixtures in the AST. Similarly, Figure 33 shows that the additional data in the HPST align decently well within the scatter from the original ignition-delay data at 10 atm. Nonetheless, in the final assessment, those data are still not included due to the increased uncertainty as to what the test temperatures and pressures actually were prior to the ignition event.

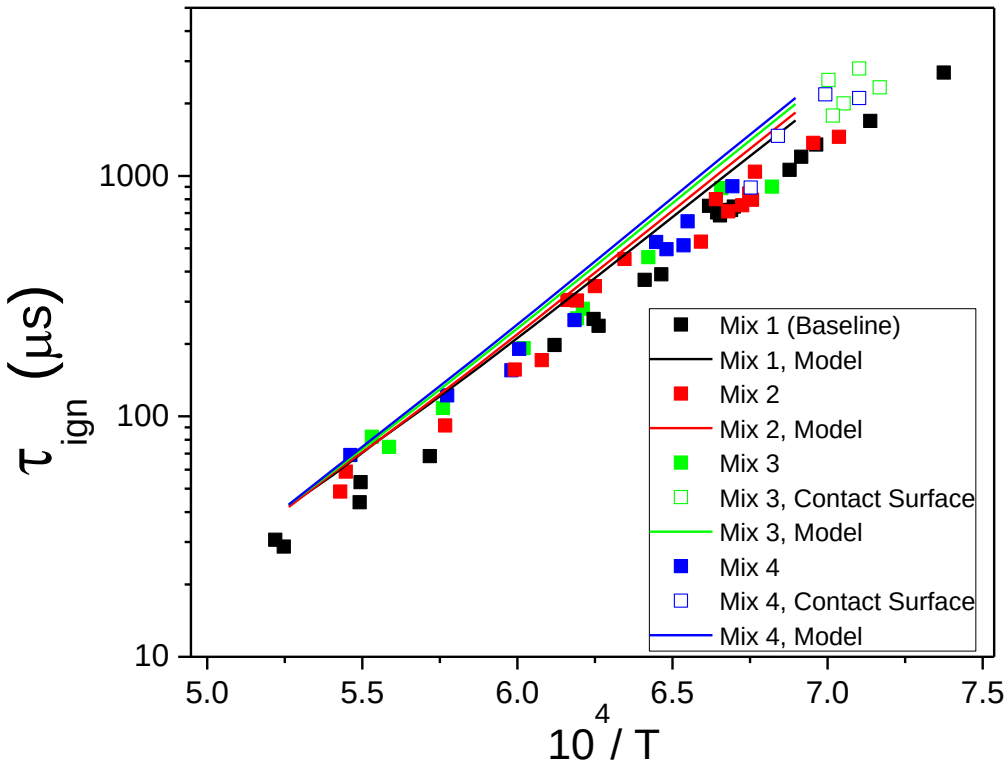

Figure 32. Ignition delay time data for all mixtures in the AST at 1.75 atm. Included for comparison are the discarded data from the experiments with a pressure drop-off (the open boxes).

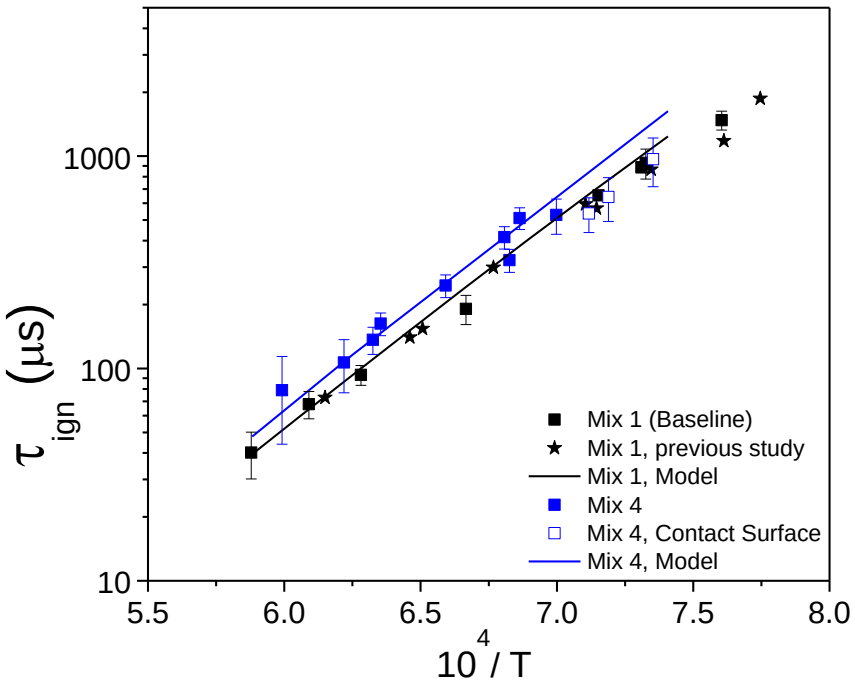

Figure 33. Ignition delay time data for all Mix 1 and 4 in the HPST at 10 atm. Included are the discarded data from the experiments with a pressure drop-off (the open boxes).

To summarize the ignition delay time results, the use of CO_2 as a replacement for N_2 in EGR-like fuel-oxidizer mixtures had little to no effect on ignition delay times. The uncertainty associated with Mix 2-4 was greater than that of Mix 1, but in the end, the results were nearly the same, if not exactly the same within the uncertainty of the experiments. In the next section, the results of a numerical investigation into the kinetics of CO_2 is given.

Modeling Comparisons, Third-Body Effects of CO_2

From the ignition delay time results in the previous section, the chemical effects of CO_2 amongst all mixtures were quite small. For each mixture, the ignition delay time data agreed well with the other mixtures (within the scatter/uncertainty of the data). This

agreement was also true for all mixtures when modeled in CHEMKIN with the Aramco 1.3 mechanism. To verify the chemical effects of CO_2 (or lack thereof), a brief numerical investigation was undertaken to examine chemical and third-body effects of CO_2.

The previous chapter briefly discussed the outcome of a sample of studies from the literature involving CO_2 in combustion. Studies that investigated EGR-related mixtures in shock tubes found that the addition of CO_2 played a negligible role in the combustion of hydrocarbons. All work done for this thesis gave similar results as the aforementioned studies, even with much higher levels of CO_2 addition. Even when CO_2 concentrations were much greater than those in [31] and [32], the ignition delay time behavior of all the investigated mixtures showed little variation, if any. This lack of variation amongst mixtures indicates that CO_2, with its high dissociation energy, was essentially non-reactive and did not contribute significantly to the formation or destruction of radical species.

To verify this negligible chemical effect, numerically, a new species with the same thermodynamic properties as CO_2, referred to as FCO_2, was introduced into the Aramco 1.3 mechanism. The addition of this species allowed any thermal and pressure/third-body effects of CO_2 to remain in the simulations, while preventing it from participating chemically. When simulations were run in CHEMKIN with Mix 4, using FCO_2 instead of CO_2, the results of this exchange showed no variation in ignition delay time behavior. Unlike in flame speed simulations, CO_2 was found to play no role chemically relating to ignition delay time and must have only participated thermally

(still being included in the energy equation to absorb thermal energy) and as a third body.

When a species behaves as a third body in a chemical reaction, it does not react, but adds or removes energy from the other species in the reaction through colliding with them. The effect of these collisions on the reaction depends upon the mixture concentration of the third body and upon the molecular size/composition of the third body itself. A parameter related to how much energy is added or removed by a third body from collisions is the third-body collision efficiency (or chaperon efficiency). The chaperon efficiency of a given third body affects the progress of a given i^{th} reaction, q_i, as follows (from the CHEMKIN theory manual, [33])

$$q_i = \left[\sum_{k=1}^{K} \alpha_{ki}[X_k]\right]\left(k_{fi}\prod_{k=1}^{K}[X_k]^{\nu_i'} - k_{ri}\prod_{k=1}^{K}[X_k]^{\nu_i''}\right) \quad (1)$$

Where X_k is the concentration of species k, k_{fi} and k_{ri} are the respective forward and reverse reaction rates for the reaction, ν_i' and ν_i'' are the stoichiometric coefficients for the respective left and right sides of the reaction, and α_{ki} is the collision efficiency for species k of the i^{th} reaction. In CHEMKIN, the collision efficiency is given a value of 1 for all species unless otherwise specified as a third body. For reactions involving a third body collision partner in the Aramco 1.3 mechanism, each third body that is able to participate in a reaction can have a different value for the collision efficiency for each reaction (although most of the reactions involving CO_2 are given a value of 2.0 from in Aramco 1.3). Upon closer examination of Eq. (1), the progress of a given reaction with third bodies depends upon the molar concentration of each species (the term in square

brackets). For an ideal gas, this term is directly proportional to the partial pressure of that component. Thus, the inclusion of a third-body collision efficiency (that is not 1.0) for a given body is analogous to changing the partial pressure of that collision partner in the first term of (1).

Since CO_2 did not react chemically, the next step in the numerical investigation was to modify the third-body collision efficiencies of CO_2 in all relevant reactions (there are 29 of them in Aramco 1.3). This process was conducted solely for Mix 4 since it had the most CO_2, and had a small but quantifiable effect upon ignition delay time over the range of temperatures investigated. Initially, all the third-body efficiencies were given values of 1.0 to investigate the effect of CO_2 having equal participation as all other species in a given reaction. The third body efficiencies for CO_2 were then given a value of 20 to determine the effect of greatly exaggerated collision efficiencies. Both alterations to the collision efficiencies of CO_2 had little effect upon the ignition delay time results, which were still within the scatter of the data from the experiments. The investigation was taken one step further, however, to determine which third-body reactions had the largest impact upon the ignition delay time results. After further examination of all reactions, the following reactions (R1-R5) were found to have the greatest impact when their collision efficiencies for CO_2 were modified.

$$O + H + M \rightleftharpoons OH + M \quad \text{R1}$$

$$HCO + M \rightleftharpoons H + CO + M \quad \text{R2}$$

$$CH3 + H(+M) \rightleftharpoons CH4(+M) \quad \text{R3}$$

$$CH3 + CH3(+M) \rightleftharpoons C2H6(+M) \quad \text{R4}$$

$$H + O2(+M) \rightleftharpoons HO2(+M) \quad \text{R5}$$

Of these five key reactions, R1 was by far the most influential, with all others having a minor effect in modifying the ignition delay time results. Although R1 was most influential, R2 and R3 still impacted the results, but only in the upper end of the temperature range. Reactions R4 and R5 had greatest impact in the lower end of the temperature range. The results of the third-body excursion are shown in Figure 34 and Figure 35. Calculated ignition delay time results from Mix 1 are also shown for comparison on each graph.

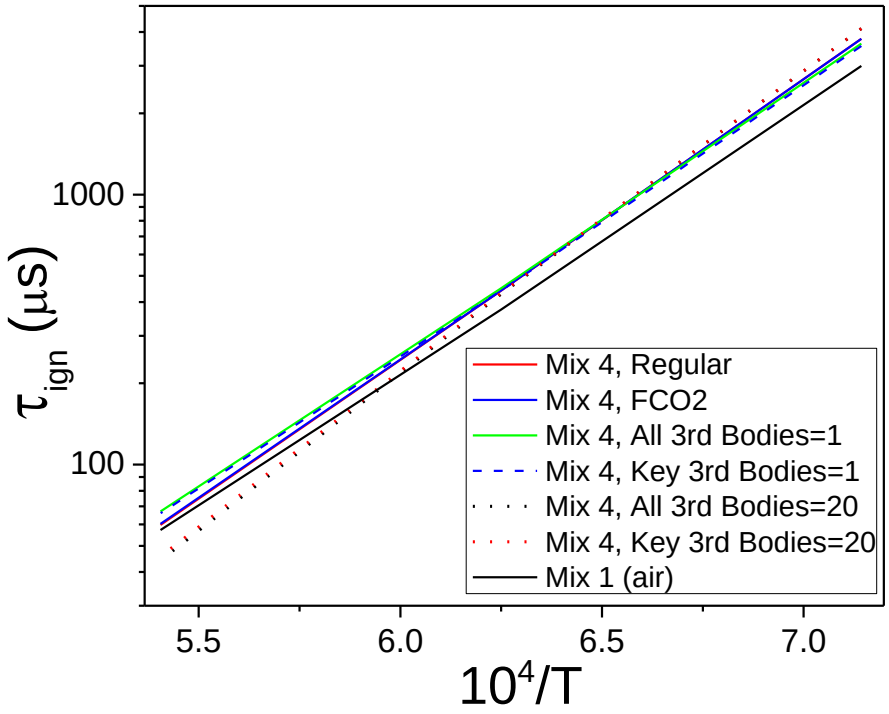

Figure 34. Modeling comparisons of third-body collision efficiencies for Mix 1 and Mix 4 at 1.75 atm.

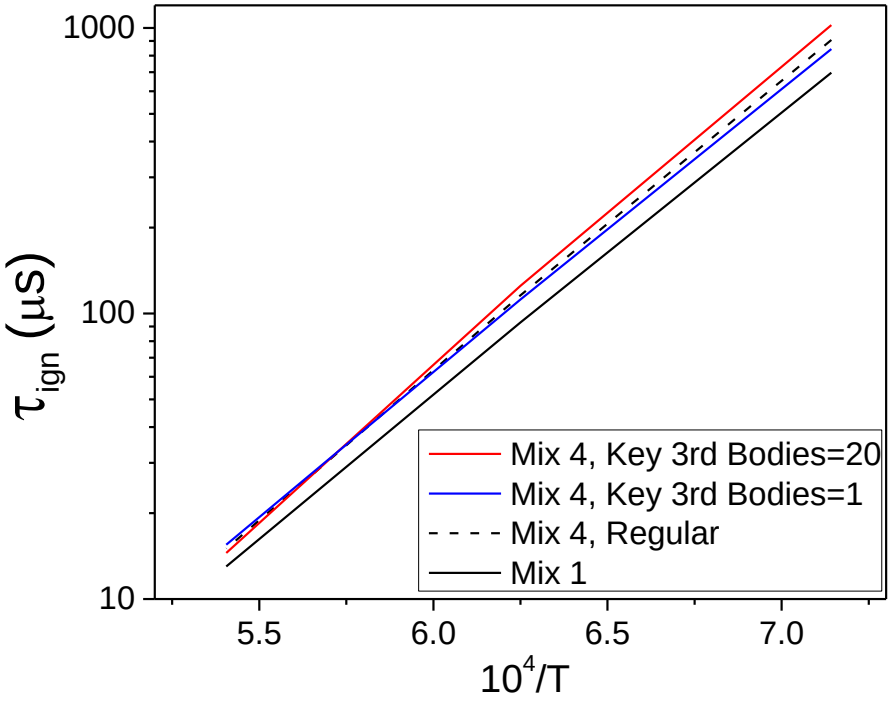

Figure 35. Modeling comparisons of third-body collision efficiencies for Mix 1 and 4 at 10 atm.

CHAPTER V

RECOMMENDATIONS AND FUTURE WORK

As is often the case in the realm of research, not all questions and areas of concern presented by this study were solved. Going forward, several issues could still be addressed to improve upon the work already accomplished. These issues need to be more thoroughly addressed before additional work is undertaken involving mixtures with high CO_2 concentrations.

The most pressing issue seems to be that of the unknown pressure expansions that prematurely end experiments. While most of the experiments provided good data, the ones with longer ignition delay times could not be used without unacceptably large amounts of uncertainty. For example, the experimental times for Mix 4 were less than half of that for Mix 1. Even Mix 2 had changes in the slope of the pressure traces around 1 ms. This shortened effective test time may not be a large problem now, but if experiments to examine the slow formation of NO_x in real EGR mixtures are to be conducted, this issue needs to be more thoroughly investigated. As previously discussed, a potential cause for this early pressure decrease is that of interactions between the reflected shock wave and the contact surface. However, from a short series of calculations, the test time observed from experiments in which a pressure drop-off occurred did not agree well with the test times calculated using shock velocities near the endwall. A potential explanation for this is a combination of incident-shock attenuation and boundary-layer growth behind the incident shock creating slower incident shocks

and the acceleration of the contact surface down the driven section (a non-linear line on an x-t diagram). Thus, a more thorough investigation into boundary-layer formation in shock tubes is needed, a problem which has otherwise been well studied. Additionally, the interaction between the boundary layer and the reflected shock needs examination. At what point does the transition to turbulence occur and how does the bifurcated reflected shock behave as it propagates into this region of transition? Were all boundary layers laminar for the low-pressure mixtures in this study (at least in the region near the endwall)? These are a sample of the questions that need more pursuit. Another avenue of investigation is that of experimental conditions behind the reflected shock wave.

Although the normal shock relations are a reliable predictor of conditions behind the reflected shock wave, the introduction of induced fluid motion can bring about questions regarding quiescence and uniformity of the bulk region behind the reflected shock. Since the measurements at the pressure transducers occur at the wall, in a region of moving fluid away from the bulk behavior behind the shock, the accuracy of P_5 conditions, and those T_5, come into question. A potential way to improve upon the monitoring of the reflected-shock conditions is by using optical thermometry. Since CO_2 has wavelengths suitable for laser absorption in the IR, this is a relatively well-known procedure in principle to measure reflected-shock temperature using the Beer-Lambert law at two different wavelengths (or lasers) simultaneously. Use of a laser setup could also give the added benefit of accurately determining passage of the reflected shock wave by visualizing the accompanying schlieren spike in the laser signal (as was done by Petersen and Hanson [10]).

As was discussed by Vivanco-Gracia in [7], many hardware upgrades need to be made to the AST facility. Though the HPST facility can be used exclusively, the AST facility gives added flexibility and is better suited for some of the optical techniques discussed in the previous paragraph. Many of the hardware issues associated with the AST are manageable, but an endwall emission diagnostic is greatly needed to improve the collection of data from experiments.

CHAPTER VI

SUMMARY

A study was conducted to investigate methane ignition in shock tubes with high levels of CO_2 dilution. The experiments were performed on the campus of Texas A&M University at the Turbomachinery Laboratory in two stainless steel shock tubes furnished with state-of-the-art measurement equipment. One tube was used for the low-pressure experiments (the AST) near 1.75 atm, while the other tube (the HPST) was used for high-pressure experiments near 10 atm. The range of mixtures tested involved methane in air at an equivalence ratio of $\phi = 0.5$. The difference between each mixture was the composition of the "air", ($0.21O_2+0.79N_2$) to ($0.21O_2+0.79CO_2$) with intermediate combinations of N_2/CO_2 in between. The temperature range over which these experiments were conducted was approximately 1400 to 1900 K.

Prior to conducting the experiments, many issues were known to the author that would cause difficulties in conducting the experiments and interpreting the data collected therefrom. The chief among them was reflected-shock bifurcation and its subsequent effects. Much fluid motion was generated, making the interpretation of pressure traces difficult. Also, the combination of pressure noise with suppressed pressure traces at ignition from increased CO_2 made interpretation of ignition delay time more difficult, but not impossible. Lastly, some of the experiments in the lower end of the temperature range provided unreliable data due to a pressure expansion occurring before ignition and prematurely ending some of the tests.

From the reliable data that were taken, ignition delay times did not vary much with mixture composition. The ignition delay time data from Mix 4 had greater uncertainty than the data from Mix 1, but the Arrhenius plots showed that the behaviors were nearly identical within the scatter of the data. Additionally, a brief numerical investigation into the kinetic and third-body behavior of CO_2 was undertaken. This investigation revealed that CO_2 has almost no chemical effect on ignition delay time in shock tubes. Additionally, the third-body collision efficiency of CO_2 was modified in all sub-reactions involving an un-reacting collision partner. Modifying CO_2's collision efficiency in these reactions from an average value of 2 up to 20 showed hardly any change in ignition delay time behavior. Thus, it can be concluded that the effect of CO_2 in these combustible shock-tube mixtures was merely thermal in nature, absorbing energy released as heat and lowering flame temperature.

A few areas showed the need for improvement upon conclusion of this study. The interaction involving the pressure drop-off needs to be investigated more thoroughly. Reflected-shock conditions are also an area of concern, since the induced fluid motion from the rear oblique shock and subsequent vortex sheet may disturb the uniformity of that region and cause the mixture to be non-homogeneous. Lastly, a few hardware components on the AST need updating to provide better data acquisition capabilities, such as an endwall window port for emission measurements.

REFERENCES

[1] ElKady, A. M., Evulet, A., Brand, A., Ursin, T. P., and Lynghjem, A., 2009, "Application of Exhaust Gas Recirculation in a DLN F-Class Combustion System for Postcombustion Carbon Capture," Journal of Engineering for Gas Turbines and Power, 131(3), pp. 0345051-0345056.

[2] Guethe, F., de la Cruz-Garcia, M., and Burdet, A., "Flue Gas Recirculation in Gas Turbine; Investigation of Combustion Reactivity and NOx Emission," Proc. ASME Turbo Expo 2009.

[3] Petersen, E. L., Hall, J. M., Smith, S. D., de Vries, J., Amadio, A. R., and Crofton, M. W., 2007, "Ignition of Lean Methane-Based Fuel Blends at Gas Turbine Pressures," Journal of Engineering for Gas Turbines and Power, 129(4), pp. 937-944.

[4] Mathieu, O., Kopp, M. M., and Petersen, E. L., 2013, "Shock-Tube Study of the Ignition of Multi-Component Syngas Mixtures With and Without Ammonia Impurities," Proceedings of the Combustion Institute, 34(2), pp. 3211-3218.

[5] Aul, C. J., Metcalfe, W. K., Burke, S. M., Curran, H. J., and Petersen, E. L., 2013, "Ignition and Kinetic Modeling of Methane and Ethane Fuel Blends With Oxygen: A Design of Experiments Approach," Combustion and Flame, 160(7), pp. 1153-1167.

[6] Petersen, E. L., Rickard, M. J. A., Crofton, M. W., Abbey, E. D., Traum, M. J., and Kalitan, D. M., 2005, "A Facility for Gas- and Condensed-Phase Measurements Behind Shock Waves," Measurement Science and Technology, 16(9), pp. 1716-1729.

[7] Vivanco-Gracia, J. E., 2014, "A New Shock Tube Facility for the Study of High Temperature Chemical Kinetics," Master of Science, Texas A&M University.

[8] Petersen, E. L., 2009, "Interpreting Endwall and Sidewall Measurements in Shock-Tube Ignition Studies," Combustion Science and Technology, 181(9), pp. 1123-1144.

[9] Mark, H., 1958, "The Interaction of a Reflected Shock Wave With the Boundary Layer in a Shock Tube," N. A. C. A. 1418, ed.Ithica, New York.

[10] Petersen, E. L., and Hanson, R. K., 2006, "Measurement of Reflected-shock Bifurcation Over a Wide Range of Gas Composition and Pressure," Shock Waves, 15(5), pp. 333-340.

[11] Strehlow, R. A., and Cohen, A., 1959, "Limitations of the Reflected Shock Technique for Studying Fast Chemical Reactions and Its Application to the Observation of Relaxation in Nitrogen and Oxygen," The Journal of Chemical Physics, 30(1), pp. 257-265.

[12] Byron, S., and Rott, N., "On the Interaction of the Reflected Shock Wave with the Laminar Boundary Layer on the Shock Tube Walls.," Proc. Proceedings of the Heat Transfer and Fluid Mechanics Institute, R. Binder, M. Epstein, R. Mannes, and H. Yang, eds., Stanford University Press, Stanford, pp. 38-54.

[13] Center, R. E., 1963, "Reflected Shock Interaction with Shock Tube Boundary Layers," Physics of Fluids, 6(2), pp. 307-308.

[14] Bull, D. C., and Edwards, D. H., 1968, "An Investigation of the Reflected Shock Interaction Process in a Shock Tube," AIAA Journal, 6(8), pp. 1549-1555.

[15] Davies, L., and Wilson, J., 1969, "Influence of Reflected Shock and Boundary-Layer Interaction on Shock-Tube Flows," Physics of Fluids, 12(5), pp. 37-43.

[16] Dyner, H. B., 1966, "Density Variation due to Reflected Shock-Boundary-Layer Interaction," Physics of Fluids, 9(5), pp. 879-892.

[17] Fokeev, V. P., and Gvozdeva, L. G., 1990, "Study of Bifurcation of Reflected Shock Waves in Channels of Various Cross-Sections," 208, pp. 862-866.

[18] Takano, Y., 1987, "Simulations for Effects of Side-Wall Boundary-Layer on Reflected-Shock Flow Fields in Shock Tubes," Shock Tubes and Waves: Proceedings of the Sixteenth International Symposium on Shock Tubes and Waves, H. Gronig, ed., VCH Publishing, pp. 645-651.

[19] H. Kleine, Lyakhov, V. N., Gvozdeva, L. G., and Gronig, H., "Bifurcation of a Reflected Shock Wave in a Shock Tube," Proc. 18th International Symposium on Shock Waves, K. Takayama, ed., Springer, pp. 261-266.

[20] G.J. Wilson, S. P. S., W.D. Gillespie, 1992, "Time-Dependent Simulation of Reflected-Shock/Boundary Layer Interaction in Shock Tubes," Shockwaves at Marseille, L. Z. D. R. Brun, ed., Springer-Verlag, Marseille, France, pp. 439-444.

[21] Weber, Y. S., Oran, E. S., Boris, J. P., and Anderson Jr., J. D., 1995, "The Numerical Simulation of Shock Bifurcation Near the End Wall of a Shock Tube," Physics of Fluids, 7(10), pp. 2475-2488.

[22] Ihme, M., Sun, Y., and Deiterding, R., 2013, "Detailed Simulations of Shock-Bifurcation and Ignition of an Argon-diluted Hydrogen/Oxygen Mixture in a Shock Tube," 51st AIAA Aerospace Sciences MeetingGrapevine, Texas.

[23] Khokhlov, A., Austin, J., Bacon, C., Aithal, S., and Riley, K., 2011, "Reflected Shock Bifurcation in a Square Channel," 49th AIAA Aerospace Sciences MeetingOrlando, Florida.

[24] Lamnaouer, M., Kassab, A., Divo, E., Polley, N., Garza-Urquiza, R., and Petersen, E., 2014, "A Conjugate Axisymmetric Model of a High-Pressure Shock-Tube

facility," International Journal of Numerical Methods for Heat & Fluid Flow, 24(4), pp. 873-890.

[25] Yamashita, H., Kasahara, J., Sugiyama, Y., and Matsuo, A., 2012, "Visualization Study of Ignition Modes Behind Bifurcated-Reflected Shock Waves," Combustion and Flame, 159(9), pp. 2954-2966.

[26] Dumitrescu, L., Popescu, C., and Brun, R., "Experimental Studies of the Shock Reflection and Interaction in a Shock Tube," Proc. Shock Tubes. Proceedings of the 7th International Shock Tube Symposium, I. Glass, ed., University of Toronto Press, Toronto, pp. 751-770.

[27] Cong, T. L., and Dagaut, P., 2008, "Experimental and Detailed Kinetic Modeling of the Oxidation of Methane and Methane/Syngas Mixtures and Effect of Carbon Dioxide Addition," Combustion Science and Technology, 180(10-11), pp. 2046-2091.

[28] Glaborg, P., and Bentzen, L. L. B., 2008, "Chemical Effects of a High CO2 Concentration in Oxy-Fuel Combustion of Methane," Energy & Fuels, 22, pp. 291-296.

[29] Halter, F., Foucher, F., Landry, L., and Mounaïm-Rousselle, C., 2009, "Effect of Dilution by Nitrogen and/or Carbon Dioxide on Methane and Iso-Octane Air Flames," Combustion Science and Technology, 181(6), pp. 813-827.

[30] Liu, F., Guo, H., and Smallwood, G. J., 2003, "The Chemical Effect of CO2 Replacement of N2 in Air on the Burning Velocity of CH4 and H2 Premixed Flames," Combustion and Flame, 133(4), pp. 495-497.

[31] Levy, Y., Olchanski, E., Sherbaum, V., Erenburg, V., and Burcat, A., 2006, "Shock-Tube Ignition Study of Methane in Air and Recirculating Gases Mixture," Journal of Propulsion and Power, 22(3), pp. 669-676.

[32] Comandini, A., Dubois, T., and Chaumeix, N., 2014, "Autoignition of n-Decane/n-Butylbenzene/n-Propylcyclohexane Mixtures and the Effects of the Exhaust Gas Recirculation," Combustion Science and Technology, 186(10-11), pp. 1536-1551.

[33] 2013, "CHEMKIN 10131," Reaction Design, San Diego.

[34] Metcalfe, W. K., Burke, S. M., Ahmed, S. S., and Curran, H. J., 2013, "A Hierarchical and Comparative Kinetic Modeling Study of C1− C2Hydrocarbon and Oxygenated Fuels," International Journal of Chemical Kinetics, 45(10), pp. 638-675.